Multi-beam echo-sounder bathymetric measurements
Implications of using frequency modulated pulses

H. Mohammadloo, Tannaz; Snellen, Mirjam; Simons, Dick G.

DOI
10.1121/1.5050816

Publication date
2018

Document Version
Final published version

Published in
Journal of the Acoustical Society of America

Multi-beam echo-sounder bathymetric measurements: Implications of using frequency modulated pulses

Tannaz H. Mohammadloo, Mirjam Snellen, and Dick G. Simons

Citation: The Journal of the Acoustical Society of America **144**, 842 (2018); doi: 10.1121/1.5050816
View online: https://doi.org/10.1121/1.5050816
View Table of Contents: http://asa.scitation.org/toc/jas/144/2
Published by the Acoustical Society of America

Multi-beam echo-sounder bathymetric measurements: Implications of using frequency modulated pulses

Tannaz H. Mohammadloo,[a] Mirjam Snellen, and Dick G. Simons
Acoustics Group, ANCE, Department of Control & Operations, Faculty of Aerospace Engineering, Delft University of Technology, 2629 HS, Delft, The Netherlands

(Received 16 February 2018; revised 16 July 2018; accepted 1 August 2018; published online 21 August 2018)

In this contribution bathymetric uncertainties induced by the use of frequency modulated (FM) signals for multi-beam-echo-sounder (MBES) measurements are quantified and their relevance for MBES bathymetric uncertainty predictions is assessed. When switching to FM, the quality of depth measurements can get deteriorated due to the Doppler effect and baseline decorrelation. The uncertainty due to the former is divided into second-order (imperfectness of the Doppler-range correction) and first-order (effect on beamsteering) effects. The latter also holds for continuous wave (CW) signals. Here, situations of relevance for measurements in the continental shelf and ship dynamics associated to rough and calm sea-states are considered, and the vertical uncertainty induced by the above sources is quantified. The influence of the Doppler effect depends on the sea state, but is found to potentially have a significant contribution to the MBES error budget for both FM and CW [nearly 82% (rough) and 68% (calm) of the total uncertainty]. The effect of baseline decorrelation depends on the actual pulse shape. For the specifications investigated, vertical uncertainties induced by this source are predicted to be larger for FM than that of CW. This is confirmed by a comparison between the modelled and measured effect on depth uncertainties when switching to FM.
https://doi.org/10.1121/1.5050816

[ZHM] Pages: 842–860

I. INTRODUCTION

Modern multi-beam echo-sounders (MBESs) have the option to use frequency modulated (FM) signals, in addition to the more standard continuous wave (CW) signals. FM signals enable emitting long pulse lengths, while keeping a high ranging resolution.[1] The latter is obtained by matched filtering the received echo signals. The long pulse length allows for measurements at larger ranges, resulting in an increase in the attainable swath. Despite the advantages gained by using FM signals, it has been observed that switching from CW to FM can result in noisier bathymetric measurements.[2–5] A number of potential sources for the degradation in the performance of bathymetric measurements due to the use of FM signals have been identified in Refs. 5–7.

The first cause is related to the Doppler effect. Since the MBES is in a constant movement, the received signals will be affected by a Doppler frequency shift. When this received Dopplerized signal is matched filtered, using as replica the emitted signal, the matched filtered output will be affected by this difference in frequency, resulting in a bias in the estimate of the arrival time. In general, this bias is corrected for in the MBES processing, using the speeds of the transducers at transmission and reception.[8] Still, the imperfect knowledge on the speeds, and thus the imperfect correction, gives rise to uncertainties in the MBES derived depths.

In addition, the frequency shift as introduced by the Doppler effect also has an impact on the beamsteering, resulting in uncertainties in the steering angle. This second effect, however, also holds for CW pulses and is in general not compensated for.[9] An uncertainty in the steering angle gives rise to uncertainties in the estimated depths which is important for the prediction of the total error budget carried out prior to a MBES bathymetric survey; an underestimation of the contribution of the Doppler effect potentially leads to an optimistic expectation of the depth uncertainties.

The second origin of potential effects on bathymetric uncertainties, stemming from the use of FM signals, is the baseline decorrelation. The phenomenon of baseline decorrelation is encountered in the MBES interferometry step, applied when using phase detection. For the interferometry step, the full MBES receiving array is divided into two sub-arrays and the phase difference of the signals arriving at the two sub-arrays is determined. The time at which the two signals are in phase is taken as the arrival time and the angle corresponding to this zero phase difference is referred to as the angle of arrival (AOA).[10] (For other systems, e.g., full interferometric systems, other effects such as footprint shift can also be important. Expressions for uncertainties in these cases, based on the Cramer-Rao lower bound, can be found, for example, in Refs. 11–14).

The backscattered signals received by these two sub-arrays are slightly different due to the different angular directions, and consequently the coherence between the two received signals is reduced. This degradation in coherence,

[a]Electronic mail: t.hajimohammadloo@tudelft.nl

negatively affecting the quality of the phase estimates, is a purely random process[15] which cannot be compensated for. This effect has been addressed in a number of studies, for example, in Refs. 15–18, for different environments; based on the different measurement configurations and signals considered, different outcomes were found regarding the importance of the baseline decorrelation. In Ref. 5 the effect was studied nicely and thoroughly specifically for the MBES using FM pulses, and expressions were derived for quantifying the uncertainty in MBES bathymetric measurements due to baseline decorrelation for both FM and CW pulses. For the situation considered in Ref. 5, consisting of a water depth of around 200 m and a 73 kHz MBES, it was found that the phase difference uncertainty (which results in bathymetry uncertainty) due to baseline correlation is higher for FM pulses than for CW pulses. This indicates that indeed the baseline decorrelation is a factor potentially contributing to a degradation in the bathymetric measurements when switching from CW to FM pulses.

In this contribution the analysis of Ref. 5 is extended to a shallow water configuration (∼60 m), of relevance to marine environments typically encountered on the continental shelf, and a high frequency MBES system (center frequency of 300 kHz). Both abovementioned contributions, i.e., the effects of Doppler and decorrelation, will be quantified for this environment. This will provide insight into their relative importance. Another important step in this paper, in addition to the analysis of Ref. 5, is to investigate if a degradation in bathymetric measurements due to the use of FM pulses is indeed expected for these types of environments. To this end, the contribution of the Doppler effect will be compared to all other uncertainties inherent to MBES bathymetric measurements, i.e., range measurement, roll and steering angle, pitch angle, beam opening angle, and sound speed profile. For this, use is made of predictions of the total propagated uncertainty based on Refs. 19 and 20. To assess the agreement of the modeled uncertainties with those encountered in measurements, depth measurements in both FM and CW modes acquired during a survey in the Westerschelde Estuary using EM2040c dual head are analyzed.

A preliminary study on the effect of using FM pulses on the uncertainty of the MBES derived depth was presented in Ref. 21, mainly investigating the sensitivity to various pulse shapes. In the present contribution, focus is on a realistic MBES so that the results can be compared with measurements. In addition, the considered uncertainties are compared to other sources of uncertainty in MBES bathymetric measurements.

This paper is organized as follows. Section II focuses on the expected effects of the use of FM signals. In Sec. III the contributions of Sec. II will be quantified for a realistic situation followed by a discussion on their relative contribution to the total bathymetric uncertainties in Sec. IV. The results from real measurements will be presented in Sec. V and the conclusions will be drawn in Sec. VI.

II. MODELING THE EFFECTS OF USING FM SIGNALS ON MBES BATHYMETRIC UNCERTAINTIES

Considering the use of either CW or FM pulse shapes, the only difference in the processing is the fact that for the FM signal, matched filtering, i.e., pulse compression, is applied at reception. This is illustrated in the diagram of Fig. 1.

The potential causes for the degradation in MBES bathymetric measurement performance due to the use of FM signals, as indicated by the ellipses in Fig. 1, are:

(1) The MBES is in constant movement. Consequently, the received signal shape will be affected by Doppler effects. When applying matched filtering to the received signal using as the replica the emitted signal without Doppler, an error will be introduced.
(2) The Doppler effect will also affect the beamsteering since the delays applied assume the frequency of the signal without the presence of Doppler. However, this effect also exists for CW signals.
(3) In the interferometry step the full array is divided into two subarrays and the phase shifts as a function of time between the beamformed signals at these two subarrays are determined. The time at which this phase shift is zero corresponds to the return from the seafloor exactly at the beam angle. The estimates of the phase shifts, and therefore the zero-crossing, are deteriorated by noise (intrinsic and additive). Whereas the improved signal-to-noise (SNR) (reduction of relative contribution of additive noise), for FM signals will reduce this noise, Refs. 5 and 6 suggested that the sidelobes of the matched filtered FM signal will increase the noise (intrinsic noise increase).

A. Effect of Doppler frequency shift on MBES bathymetric measurements

In this subsection, the effect of the Doppler frequency shift on the MBES measurements is addressed, thereby quantifying the effects indicated by numbers 1 and 2 in Fig. 1.

The Doppler frequency shift stems from the movement of the MBES transducer when emitting and receiving the signal. Consider a location on the seafloor at the angular position θ, see Fig. 2 (for the moment, assume that the across track angle under which the MBES is mounted on the ship and the roll angle are zero). The distance between the two sub-array centers (hereafter denoted a and b) is denoted by L. The speeds of the array center at emission and reception projected on the beam direction are v_e and v_r, respectively. It is assumed that there is no rotation around the array center.

The time difference between emitting and receiving the first sample of the emitted pulse for a receiver located at the center of the array is denoted by τ. Since the signal samples span the pulse length and the receiver and transmitter are in

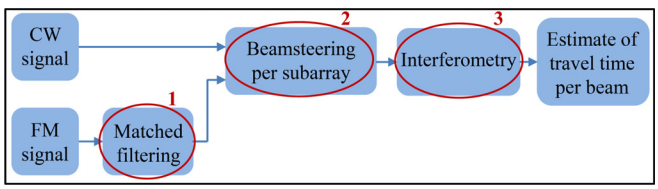

FIG. 1. (Color online) Flow diagram of the MBES processing chain. Indicated with ellipses are the three processing steps that are considered in this paper with respect to potential influence of the use of an FM pulse on the quality of the MBES derived estimates of water depths.

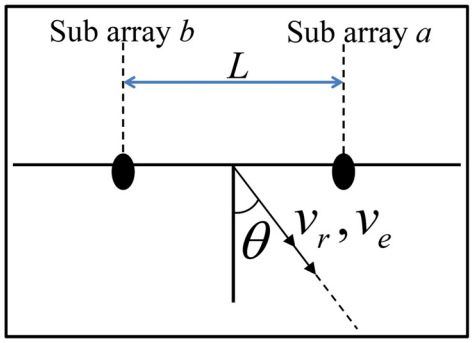

FIG. 2. (Color online) Geometrical configuration considered. The figure is based upon figures from Ref. 5.

movement over the pulse length, the time needed for the signal to travel from source to receiver changes over the pulse length.

Consider now the signal sample received at the instant t_r, which corresponds to the signal sample transmitted at the instant t_e where both times are defined as the elapsed time since the start of the transmission. The following equations relate these two instances for the two subarrays a and b, respectively:

$$c(t_r - t_e) = c\tau - v_e t_e - v_r(t_r - \tau) - \frac{L}{2}\sin\theta, \tag{1}$$

$$c(t_r - t_e) = c\tau - v_e t_e - v_r(t_r - \tau) + \frac{L}{2}\sin\theta, \tag{2}$$

with c being the speed of sound in the water and assuming a sufficiently large water depth to allow for neglecting the curvature of the wave front. For the array center and $t_e = 0$, one finds $t_r = \tau$, i.e., the two-way travel time of the first sample from and to the array center. For all subsequent times, the above expressions model the change in the received signal due to the movement of the transducer at emission and reception. Using the above equations, the received signals can be expressed as[5]

$$s_a(t) = s\left(\frac{k_{r1}}{k_e}(t-\tau) + \frac{1}{k_e}\frac{L\sin\theta}{2c}\right) \quad \text{with}$$
$$k_e = 1 - \frac{v_e}{c} \quad \text{and} \quad k_{r1} = 1 + \frac{v_r}{c}, \tag{3}$$

$$s_b(t) = s\left(\frac{k_{r2}}{k_e}(t-\tau) - \frac{1}{k_e}\frac{L\sin\theta}{2c}\right) \quad \text{with } k_{r2} = 1 + \frac{v_r}{c}, \tag{4}$$

with s the emitted signal shape. It is seen that the received signals are delayed and distorted, i.e., affected by Doppler, versions of the transmitted signal.

1. Doppler effect on matched filtered signals

The resulting Doppler frequency shift will affect the matched filtering output. Small Doppler mismatches, where the matched filtered signal is Doppler shifted but the replica is not, do not change the general matched filter output shape and reduce the amplitude very little for FM pulses.[22] However, the maximum of the matched filter output is shifted in time. Thus, uncompensated Doppler frequency shifts change the estimate of the two-way travel time; this is the so-called range-Doppler coupling[23]

$$t^{shift} = -f_d\frac{T}{B}, \tag{5}$$

where t^{shift} indicates the shift in the location of the maximum of the matched filter output with respect to the undopplerized matched filter output. f_d is the difference between the frequency of the received and emitted signals (reflecting the Doppler effect) equaling $f_d = f_c(1 + v_r/c)(1 - v_e/c)^{-1} - f_c \approx f_c(v_r + v_e)/c$, where f_c is the center frequency of the signal. B and T are the signal bandwidth and pulse duration, respectively. It is assumed that the MBES transducer speeds are much smaller than c. In case the exact value for f_d is considered instead of the approximation, the resulting t^{shif} will be in agreement with Ref. 24.

The maxima of signals y_a and y_b are thus shifted with shifts $t_{y_a}^{shift}$ and $t_{y_b}^{shift}$ of

$$\delta t = t_{y_a}^{shift} = t_{y_b}^{shift} = -\frac{v_e + v_r}{c} f_c \frac{T}{B}, \tag{6}$$

where δt corresponds to the expected shift in the estimate for the two-way travel time. Thus, the first impact of the Doppler effect is a time shift in the estimated arrival time, and thus the estimated range $\delta r = -f_c T(v_e + v_r)/(2B)$. In principle, the time shift (range error) due to the range-Doppler coupling can be compensated in the post-processing mode if the speeds are known.[8,25] However, an uncertainty in these speeds results in an uncertainty in the correction applied, leading to an uncertainty in the estimated bathymetry.

2. Doppler effect on beamforming

When beamforming, the signals as received on the different receiving elements are delayed and then summed. The delay is such that it reflects the expected differences in the arrival times for the different receiving elements. The delay can be either applied on the signals in the time or frequency domain. The latter corresponds to applying a phase shift. Movement of the transducer affects the received pulse. Not accounting for this in the time delay or phase shift will, in turn, have an influence on the beamforming output. This effect exists both for FM and for CW pulses.

The derivations below consider the array to consist of two elements (a and b). For the times at which the signals are received at subarrays a and b, we can write

$$\textbf{Subarray } \boldsymbol{a}\textbf{:}\ t_r(c + v_r) = t_e(c - v_e) + \tau c + \tau v_r - \frac{L}{2}\sin\theta$$
$$\Longleftrightarrow t_r = \tau + t_e\frac{c - v_e}{c + v_r} - \frac{L}{2}\frac{\sin\theta}{c + v_r}, \tag{7}$$

$$\textbf{Subarray } \boldsymbol{b}\textbf{:} t_r(c + v_r) = t_e(c - v_e) + \tau c + \tau v_r + \frac{L}{2}\sin\theta$$
$$\Longleftrightarrow t_r = \tau + t_e\frac{c - v_e}{c + v_r} + \frac{L}{2}\frac{\sin\theta}{c + v_r}. \tag{8}$$

The first term in the expression for t_r is the time between the emission of the first signal sample and its arrival at the full array center. The term in the middle indicates the compression or expansion of the signal corresponding to the Doppler shift in frequency. The last term of these two equations indicates the time shifts that need to be applied when steering in direction θ. However, the time delays applied in the MBES are different and do not account for the speed of the transducer, i.e., they account only for the speed of sound c and not for the full $(c + v_r)$ terms, resulting in a difference between the steering angle aimed for and that obtained (θ_s). The following holds:

$$\frac{L\sin\theta_s}{c} = \frac{L}{2}\frac{\sin\theta}{c+v_r} + \frac{L}{2}\frac{\sin\theta}{c+v_r} \iff \sin\theta_s \approx \sin\theta\left(1-\frac{v_r}{c}\right). \tag{9}$$

The term $1 - v_r/c$ is derived using the Taylor series expansion of $1/(1 + v_r/c)$ with $|v_r/c| \ll 1$ around the point zero, truncated after the first-order term. Using the Taylor series expansion of $\sin^{-1}[\sin\theta(1 - v_r/c)]$ around the point $\sin\theta$, again truncated after the first order term, results in the following expression for the error in the steering angle

$$\delta\theta_s = \theta_s - \theta \approx -\frac{1}{\sqrt{1-\sin^2\theta}}\frac{v_r}{c}\sin\theta = -\frac{v_r}{c}\tan\theta. \tag{10}$$

This bias is equal for CW and FM signals. In contrast to the effect of Doppler on the matched filtered signals which is often taken into account in the post processing, the angular bias in the beamsteering is not corrected for.[9] This bias in the angle estimate varies from ping to ping and is as such in this research considered as a contribution to the depth uncertainty considering v_r as the random variable.

3. Doppler effect on MBES bathymetric measurements

Finally, the uncertainty in the bathymetric measurements as introduced by the Doppler frequency shift can be determined from the following expression:

$$d = r\cos P\cos(\theta_s + R + \theta_{\text{mount}}) = r\cos P\cos\theta, \tag{11}$$

where d and θ_s are the depth below the transducer at the instant of the measurements and steering angle relative to the transducer normal, P is the pitch angle, R is the roll, and θ_{mount} is the across track angle under which the MBES is mounted on the ship. The angle θ is defined as $\theta_s + R + \theta_{\text{mount}}$ and is the beam angle with respect to the depth-axis. r is the oblique distance between the transducer and seafloor.

In case there is an error in the steering angle due to the Doppler effect, $\sigma^2_{\theta_{s,\text{Doppler}}}$, an uncertainty in the bathymetry, $\sigma^2_{d,\theta_{s,\text{Doppler}}}$, is introduced. The expression for the contribution of this error is

$$\begin{aligned}\sigma^2_{d,\theta_{s,\text{Doppler}}} &= (r\cos P\sin\theta)^2\sigma^2_{\theta_{s,\text{Doppler}}}\\ &= (r\cos P\sin\theta)^2\frac{\text{var}(v_r)}{c^2}\tan^2\theta,\end{aligned} \tag{12}$$

where $\sigma^2_{\theta_{s,\text{Doppler}}}$ is determined by applying error propagation to Eq. (10) and $\text{var}(v_r)$ denotes the variations in the speed at the reception which in this case corresponds to the variance of v_r.

Similarly, an error in the estimate of the range shift due to the Doppler effect (stems from the errors in the estimate of the transducer speeds), $\sigma^2_{r_{\text{Doppler}}}$, results in a bathymetric uncertainty $(\sigma^2_{d,r_{\text{Doppler}}})$. For the bathymetry uncertainty we have

$$\begin{aligned}\sigma^2_{d,r_{\text{Doppler}}} &= (\cos P\cos\theta)^2\sigma^2_{r_{\text{Doppler}}}\\ &= (\cos P\cos\theta)^2\left(f_c\frac{T}{\sqrt{2}B}\right)^2\sigma^2_{v_r}.\end{aligned} \tag{13}$$

Here, it is assumed that the uncertainty in the speed at transmission and reception are equal and $\sigma^2_{v_r}$ denotes the uncertainty in the speed at the reception. This is a valid assumption for the situations where the two-way-travel-time is short compared to the typical period of change in the wave motion [the ocean wave period spectra is larger than 4 s (Refs. 26, 27)] and thus the speeds at transmission and reception are almost equal. However, in the deeper water when the two-way-travel-time can be several seconds, these speeds are different and the error propagation should be applied separately to them. $\sigma^2_{d,r_{\text{Doppler}}}$ only occurs when using FM pulses. However, the bathymetric uncertainty induced by the error in the beamsteering angle, Eq. (12), holds for both CW and FM pulses.

B. Effect of baseline decorrelation on MBES bathymetric measurements

Signals arriving from scatterers located in the signal footprint (instantly ensonified area) overlap in time, i.e., the signals received at one instant of time result from contributions of all scatterers within the signal footprint. Hence, the footprint can be considered as a source dimension with its own directivity pattern. This fluctuation and the fact that the two sub-arrays observe the bottom along slightly different angular directions result in a decorrelation between the two received signals. This decorrelation is referred to as baseline decorrelation which is an intrinsic noise origin (inherent component of the acoustical signal),[28] and increases as the size of the footprint gets larger (due to the more fluctuating directivity pattern). It has been suggested that due to the presence of sidelobes in the matched filtered FM pulse, its footprint gets larger compared to that of CW, and hence the baseline decorrelation increases.

Reference 20 accounts for the depth uncertainty induced by the interferometry step (phase detection) through an uncertainty in the angle estimate as the following:

$$\sigma^2_{d,\theta_{\text{meas}}} = (r\cos P\sin\theta)^2\sigma^2_{\theta_{\text{meas}}}, \tag{14}$$

where the depth uncertainty due to the baseline decorrelation $(\sigma^2_{d,\theta_{\text{Decorr}}})$ is taken into account through $\sigma^2_{\theta_{\text{meas}}}$, i.e., a random error in the measurement of the impact angle which in case of phase detection reads as

$$\sigma^2_{\theta_{\text{meas}}} = \left(\frac{0.2\psi_y}{\sqrt{N}}\right)^2, \tag{15}$$

where ψ_y is the beam opening angle in the across-track direction in case no steering is applied. N is the number of phase samples defined as

$$N = \frac{\psi_y d \tan\theta}{\Delta r_p \cos\theta}, \tag{16}$$

with Δr_p being the phase sampling resolution in meters.

An alternative approach is to account for the baseline decorrelation through an uncertainty in the estimate of the phase difference zero-crossing (in the interferometry step). In the present contribution, use is made of the coherence coefficient μ (see Refs. 5, 6, and 16) for the MBES interferometry step

$$\mu = \frac{FT|s(t)|^2\left(f_c\frac{L}{2d}\frac{\cos^2\theta}{\tan\theta}\right)}{FT|s(t)|^2(0)}, \tag{17}$$

where FT denotes the Fourier transform of the signal s. s may be the actual envelope of the narrow-band signal (CW) or the envelope obtained after pulse compression of the modulated signal (FM). As the coherence coefficient is dependent on the signal parameters (shape and f_c), it is not known beforehand how this decorrelation affects CW signals compared to FM signals.

From Ref. 29, the following expression for the variance of the phase difference is obtained:

$$\sigma^2_{\Delta\phi} = \frac{1-|\mu|^2}{1-(|\mu|\cos\psi)^2}\left(\frac{\pi^2}{4} - \pi\sin^{-1}(|\mu|\cos\psi) + \left(\sin^{-1}(|\mu|\cos\psi)\right)^2\right) + \frac{1}{2}\sum_{i=1}^{\infty}\frac{1-|\mu|^{2i}}{i^2}, \tag{18}$$

where $|\mu|$ is calculated from Eq. (17) and ψ is the phase of the expected value of $s_a s_b^*$ (zero at the instant of detection) with * being the complex conjugate.

The expression for the bathymetric uncertainty induced by the errors in the time estimate due to the baseline decorrelation ($\sigma^2_{d,t_{\text{Decorr}}}$) is[5]

$$\sigma^2_{d,t_{\text{Decorr}}} = \frac{(d\sigma_{\Delta\phi})^2}{\left(2\pi f_c\frac{L\cos\theta}{c\tan\theta}\right)^2 N}. \tag{19}$$

Typically Eq. (14) or Eq. (19) can be used to account for the bathymetric uncertainty induced by interferometry. We now investigate to what extend they agree. Substituting Eq. (15) in Eq. (14) with the across-track beam opening angle (with zero steering) equaling $\psi_y = \lambda/L_{\text{array}} = c/(f_c L_{\text{array}})$, where L_{array} denotes the total length of the acoustic array which is different from the baseline length (L). The latter is chosen to be 1/3 of the total array length.[5] This substitution leads to the following expression:

$$\sigma^2_{d,\theta_{\text{meas}}} = \frac{(0.2d)^2}{\left(3f_c\frac{L}{c\tan\theta}\right)^2 N}. \tag{20}$$

It is clear that Eqs. (19) and (20) are in agreement [the part $d^2/(f_c L\sqrt{N}/c\tan\theta)^2$ is similar in both expressions], except for a coefficient Q. In the case where Eqs. (19) and (20) are used, the factor Q equals $\sigma_{\Delta\phi}/(2\pi\cos\theta)$ and $0.2/3$, respectively. $\sigma_{\Delta\phi}$ is dependent on the pulse shape. In Sec. IV the agreement between both expressions is quantified.

An additional point to highlight is the effect of additive noise. The above considerations have not taken into account the deteriorating effect of additive noise affecting the outer beams. The nature of the additive noise makes its prediction complicated (see Ref. 30), requiring information on the acoustic backscatter returned to the MBES. The backscatter strength returned to the sonar is the result of a complex interaction of the acoustic pulse transmitted and the often inhomogeneous seafloor (see as an example Refs. 31 and 32). The nature of the energy returned carries important information about the seafloor characteristics and physical properties and can be used for seafloor classification.[33,34] However, the backscatter strength might not be known before the data acquisition and no closed form expressions can be derived. Still, in Secs. III and IV, the total coherence coefficient due to both noise origins is assessed to obtain insight into the impact of additive noise. Additionally, this uncertainty source is also discussed in Sec. V, where real measurements acquired in the FM and CW modes are analyzed.

III. QUANTIFYING THE CONTRIBUTION OF THE EFFECTS OF DOPPLER AND BASELINE DECORRELATION TO MBES BATHYMETRIC UNCERTAINTY

This section aims at the quantification of the potential effects of the Doppler frequency shift and baseline decorrelation on the bathymetric uncertainty. The situation considered is that of 60 m water depth, and a high-frequency MBES (300 kHz). The MBES considered reflects the EM2040c dual head. Currently, this system is in widespread use for monitoring continental shelf waters. CW and FM specifications and the characteristics of the Kongsberg EM2040c MBES are presented in Tables I and II, respectively.[35] The modelling is carried out for the medium and very long CW pulse lengths available in EM2040c, i.e., 0.145 and 0.6 ms. The former is often used for shallow waters and the latter is employed here to assess the impact of lengthening the pulse (and consequently the footprint). For the FM, a pulse of 3 ms is considered.

For the CW pulse, a Hanning function is applied. With regards to the tapering value of the FM signal, Kongsberg considers a varying tapering value between 10% and 50%.[9] In this contribution, the modelling has been carried out using the smallest (nearly rectangular shape) and largest tapering values to assess the effect of signal smoothing.

With regards to the bandwidth used, the EM2040c transmits FM pulses with the effective bandwidth of a few kHz.[9] Here, we focus on an effective bandwidth of 2.615 kHz (see Table I). The length of the baseline is assumed to be 0.12 m

TABLE I. CW and FM specification for EM2040c.

Parameter	CW	FM
Tapering value (%)	100	10 and 50
Center frequency (kHz)	300	300
Pulse length (ms)	0.145 and 0.600	3
Effective bandwidth (kHz)		2.615

which is one-third of the theoretical array length (based on the beam opening angle), corrected for the shading (20%).

A. Effect of the Doppler frequency shift on bathymetric uncertainty

For modeling the effects of the Doppler frequency shift, the uncertainty and variance in the speeds of the MBES transducer at transmission and reception are needed. To this end, positioning and attitude data acquired during two measurement campaigns were used. One data set was acquired at the North Sea (Cleaver Bank area) on 5th of November 2013 in rough weather conditions. To assess the impact of the weather condition on the Doppler effect, we also analyzed the data set from the Plymouth Sound area, United Kingdom, acquired on the 14th of October 2004 in a calmer weather condition compared to the Cleaver Bank data. The water depth assumed for the predictions of the Doppler induced depth uncertainty was 60 m, i.e., relatively shallow water.

Shown in Fig. 3(a) is the variation of the speeds at transmission projected on the beam direction for different beam angles over a sailing track with relatively constant heading for the rough (dark color) and calm (light color) sea states. The reason for considering one track line with constant heading and not the full surveyed area is that for the projection of the speeds on the beam direction, the rotation from the navigation frame to vessel frame is required, which can significantly vary when making turns and changing sailing direction.[25] The impact of the weather condition is clearly visible. Rough weather conditions result in larger variations of the projected speeds over the varying beam angles compared to calm conditions. Larger values for calm sea state for the beams close to the nadir are due to the higher vessel speed during the data acquisition (4.63 m/s for calm and 3.06 m/s for the rough sea state). It is also seen that the variations of the speeds projected are not perfectly symmetric with respect to the nadir (this behavior was also observed in Ref. 25) for either data sets due to the vessel rolling during data acquisition (this has been confirmed by obtaining symmetric variations over the beam angles from a simulation with zero roll).

TABLE II. Characteristics of a EM2040c dual head used as input for the predictions of MBES inherent depth uncertainties.

Parameter	Value
Number of beams	400
Beam spacing mode	equi-angular
Swath width (deg.)	130
Mounting angle of transducer (deg.)	34.73 for starboard, 35.29 for port
Beam steering reference angle (deg.)	0
Along-track opening angle (deg.)	1
Across-track opening angle (deg.)	1
Range sampling resolution (m)	0.018
Phase sampling resolution (m)	0.018

As mentioned, for the bathymetric errors due to imperfect corrections of the Doppler effect in the matched filtering process, the uncertainty in the estimate of the speeds is required. To obtain an estimate for this value, a Monte Carlo simulation has been run where the projected speeds are calculated assuming the motion and positioning sensors and alignment measurements are normally distributed with the standard deviation specified by Kongsberg to meet the accuracy requirement of the EM2040c system.[36] The uncertainties of roll, pitch, heading, and heave are considered equal to 0.02°, 0.05°, 0.2°, and 0.05 m or 5% of the depth, whichever is highest, respectively. Moreover, the accuracy of transducer and motion sensors alignment are assumed to be 0.02, 0.02, 0.005 m and 0.05, 0.05, 0.05 m in the vessel coordinate system with positive x to the bow, positive y to the starboard, positive z to downward, respectively. Shown in Fig. 3(b) are the uncertainties in the estimate of the speeds for both sea states. It is seen that for the rough conditions, the uncertainties are in general higher than those of the calm.

Using these variations and uncertainties of the speeds, the MBES bathymetric uncertainty induced by the uncertainty in the Doppler effect is calculated using Eqs. (12) and (13). It should be noted that theoretically the calculation of the depth uncertainty induced by the imperfect Doppler correction requires both the uncertainties in the estimate of the speeds at transmission and reception, see Eq. (6). However, with water depth of around 60 m, the maximum TWTT for the most outer beam (65°) is approximately 0.2 s which is considerably shorter than the typical period of the waves (around 4 s) and the speeds at the reception and transmission are thus almost equal. This has also been verified from the two data sets. Figure 4 shows the resulting bathymetric uncertainty, referred to as the random vertical uncertainty (RVU), for CW and FM pulses. Although when using a CW pulse, matched filtering is not applied, the variations of the speeds still induce an error in the measurements. In this case, there is an error in the beam steering angle which is currently not corrected for in the MBES processing. It is seen that for the calm sea state, the depth uncertainty for the CW pulse is nearly 85% of that of the rough sea state for the outer most beams.

For the FM pulse there is, in addition to the error in the beam angle, also an uncertainty in the travel time estimation. The error due to beam steering (dashed curves) is independent of the pulse shape and is equal for both CW and FM pulses. However, the vertical uncertainty due to the imperfectness of Doppler range correction occurs only for FM pulses [dotted curves in Fig. 4(b)] and depends both on the bandwidth and pulse length of the signal. Widening the bandwidth (or increasing the tapering value) of the FM pulse decreases the contribution of this error source. Compared to the depth uncertainty due to the beamsteering which is a first-order effect, the contribution of the error due to the imperfectness of the Doppler range bias estimation, a

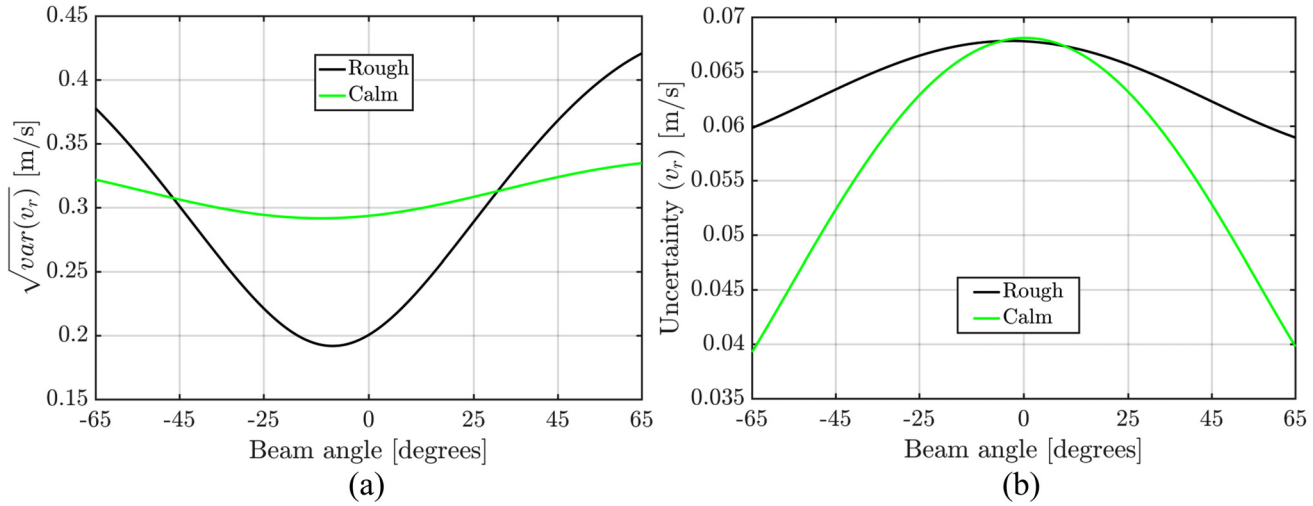

FIG. 3. (Color online) (a) Square root of the variations and (b) uncertainties in the estimate of the speeds at transmission projected on the beam direction for different beam angles for rough [dark (black)] and calm [light (green)] sea states.

second-order effect, is much smaller. Both effects and their sum are shown for FM, see Fig. 4(b). As expected, the rough sea state worsens the situation, i.e., for the outer most beams the uncertainty is increased by a factor of 1.2 and the dominant contributor is the error due to the beamsteering. It should be noted that not accounting for the Doppler effect in the matched filtering would increase this contribution typically by a factor of 10.

B. Effect of the baseline decorrelation on bathymetric uncertainty

Equations (17) and (18) are used to calculate the coherence coefficient, Fig. 5(a), and the standard deviation of the phase difference between the subarrays a and b over the phase ramp, Fig. 5(b), as a function of the beam angle, respectively.

As can be seen for the CW pulse with the duration of 0.145 ms, the coherence coefficient is the highest leading to the lowest noise over the phase ramp (dashed curves in both frames of Fig. 5). However, an increase in the pulse length leads to a decrease in the coherence coefficient and increase in the standard deviation of the phase estimate, as seen for the two CW pulses with different durations. This can be explained by the increasing signal footprint and the resulting decreasing coherence level.

With regards to the FM pulse, the coherence coefficient (and the noise over the phase ramp) is more controlled by the bandwidth and the tapering values instead of the pulse length. Increasing the tapering value results in an increase in the coherence coefficient (decrease in the noise over the phase ramp) as the sidelobe's level is reduced. Moreover, widening the effective bandwidth of the FM signal, again leads to an improvement in the coherence coefficient which is expected as the effective pulse length decreases (compare the three FM pulses in both frames of Fig. 5). An increase in the pulse length of the FM signal while the effective bandwidth and the tapering coefficient remain unchanged does

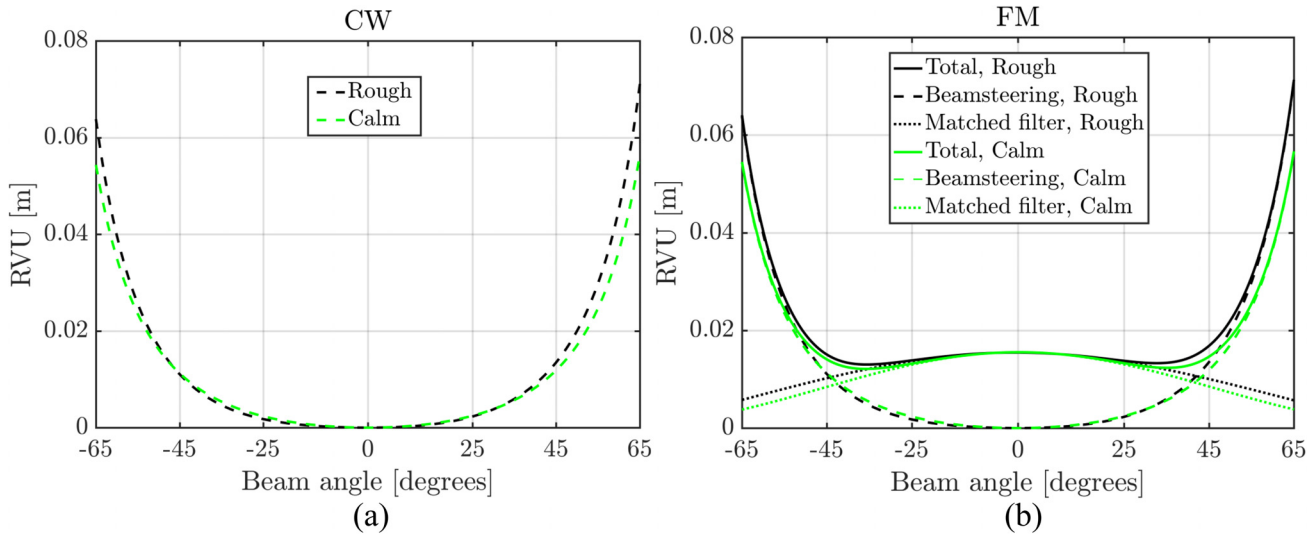

FIG. 4. (Color online) (a) bathymetric uncertainty (RVU) due to the uncertainty in the beam angle, induced by the varying Doppler frequency shift, for the CW pulse with the duration of 0.145 ms and (b) bathymetric uncertainty due to the Doppler frequency shift for the FM pulse with the effective bandwidth of 2.615 kHz and pulse length of 3 ms for a rough [dark (black)] and more calm [light (green)] sea states.

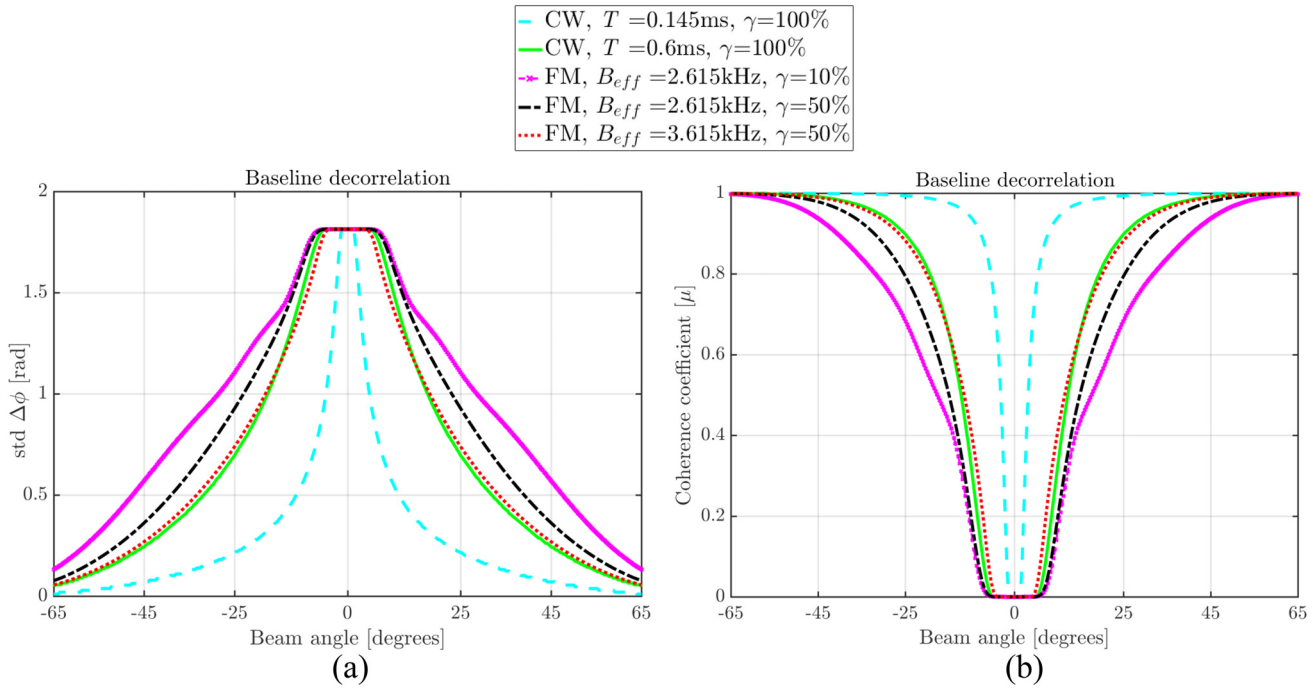

FIG. 5. (Color online) (a) coherence coefficient considering the baseline decorrelation and (b) predictions of $\sigma_{\Delta\phi}$ due to the baseline decorrelation for CW and FM pulses with different specifics. For the echo sounder a baseline L of 0.12 m was used ($\psi = 0$).

not affect the coherence coefficient. This is due to the equal pulse lengths of the two pulse-compressed signals and, consequently, equal footprints and coherence coefficient.

The comparison between the coherence level of CW and FM pulses due to the baseline decorrelation reveals that, for an effective bandwidth of 2.615 kHz and both tapering values, the coherence coefficient of the CW pulse is higher than that of FM. However, the coherence level and consequently noise over the phase ramp do fully depend on the pulse specifications and are not solely a matter of using CW or FM pulses. As an example, if we consider the FM pulse with a tapering value and effective bandwidth of 50% and 3.615 kHz (dotted curves), respectively, the coherence level due to the baseline decorrelation becomes very close to that of the CW pulse with a pulse length of 0.6 ms.

Although smoothing the FM signal and shortening the CW pulse improve the coherence coefficient, it also reduces the transmitted energy level and hence SNR is deteriorated. As mentioned in Sec. II, modelling the SNR (additive noise contribution) prior to the survey is a complicated task requiring information on bottom characteristics. However, to obtain insight into the impact of the SNR on the standard deviation of the phase difference, a simulation has been performed. The SNR modelling is carried out using the well-known active sonar equation[30] assuming a maximum transmitted energy level of EM2040c available (equaling 204.5 μPa@1 m[37]) and a sandy mud bottom. The total backscatter strength is modelled as the result of a contribution from volume backscattering and rough interface backscattering.[38] It can be shown that the total coherence coefficient is the product of baseline decorrelation coherence coefficient and additive noise coherence coefficient.[5,39] The standard deviation of the phase estimate is now derived substituting this total coherence coefficient in Eq. (18).

Shown in Fig. 6 is the standard deviation of the phase estimate resulting from both additive noise and baseline decorrelation. It is seen that for the CW pulse with the longer pulse length, the standard deviation of the phase difference is affected by the additive noise for a smaller range of outer beams. This is due to the higher target strength (increased by an increase in the ensonified area) and lower noise level (inversely proportional to the signal duration). For the two

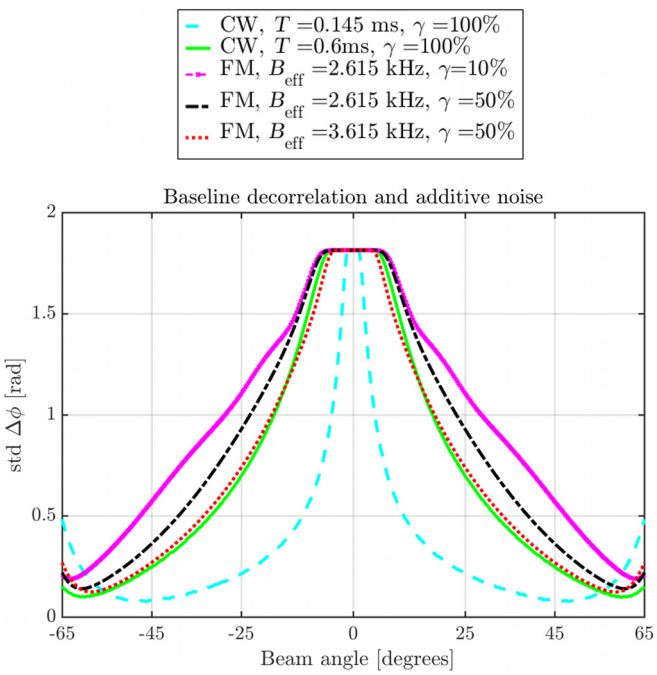

FIG. 6. (Color online) Predictions of $\sigma_{\Delta\phi}$ due to the baseline decorrelation and additive noise for CW and FM pulses with different specifics. For the echo sounder a baseline L of 0.12 m was used ($\psi = 0$).

FM pulses with the same tapering coefficients, the additive noise deteriorates the uncertainty in the phase estimate for the outer beams in a similar manner. With regards to the FM pulse with 10% tapering value (nearly rectangular) an increase in the uncertainty of the phase estimate due to the additive noise occurs for a negligible range of outer beams compared to the two other FM pulses considered, which is due to a less smooth signal. Thus, it is seen that although using a smoother FM pulse shape increases the uncertainty on the phase estimate for the outer beam due to the reduced SNR, it decreases the uncertainty due to the baseline decorrelation, and hence a trade-off has to be found between the sidelobes' reduction achieved at the cost of an increase in the additive noise.

The final bathymetric uncertainty due to the baseline decorrelation is determined using Eq. (19) and is shown in Fig. 7(a). From this figure, but also from those shown previously, it is clear that the effect of baseline decorrelation on the bathymetric uncertainty is based on the pulse shape and is not solely a matter of using a FM or CW pulse; compare the FM pulse with the largest effective bandwidth and CW pulse with the longest duration. Moreover, the bathymetric uncertainty due to the baseline decorrelation increases up to a certain beam angle and then decreases. Depending on the pulse specifications, the standard deviation of the phase difference is nearly constant for the range of beam angles. The denominator Eq. (19) thus plays an important role for the beam angles within this range and controls the shape of the bathymetry uncertainty curve (the denominator decreases with the beam angle and consequently the depth uncertainty increases). However, for the beam angles out of this range, the standard deviation decreases rapidly and the rate of its decrease is more dominant than the decreasing rate of the denominator.

To obtain the total depth uncertainty induced by the errors in the detection instant for the different pulses, the signal pulse length has to be also taken into account. This is due to the inability to separately distinguish instantaneous contributors located within the resolution cell (delimited by the pulse duration) as they are all received at the same time.[28] This means that at a given instant of reception relative to the transmission (t), the target echo contains simultaneous contributions from all scatterers included inside a resolution cell, which is determined by the pulse length. Inside this resolution cell, the instantaneous contributors cannot be distinguished separately. Under the assumption of uniformly distributed contributors within the resolution cell (which is a valid assumption if geometrically equidistributed scatterers are considered),[28] the uncertainty in the estimation of the arrival time is $T/\sqrt{12}$ (classical result for a uniform distribution[40]). Considering r in Eq. (11) as the multiplication of the sound speed and the TWTT divided by 2 and application of the error propagation gives the estimate of the induced uncertainty due to this contributor as $cT\cos P\cos\theta/(4\sqrt{3})$, and its square is added to Eq. (19). The combined depth uncertainty due to the baseline decorrelation and signal duration is shown in Fig. 7(b). It is seen that for the CW pulse with the shortest and longest durations, the vertical uncertainty due to the error on the detection instant is the lowest and highest, respectively. For the two FM pulses with different tapering values, the depth uncertainty is nearly the same. However, as the effective bandwidth increases, the uncertainty decreases. Although the depth uncertainty due to the baseline decorrelation for the FM pulses with the smaller effective bandwidth is higher than that of the CW pulse with the duration of 0.6 ms, the depth uncertainty due to the error in the detection instant of the former is lower than that of the latter. This is due to the fact that for the FM signal, the pulse length after the matched filtering is used to determine the contribution of the signal duration in the detection instant which is much smaller than the original pulse length of the FM (3 ms) and CW with the pulse length of 0.6 ms.

Shown in Fig. 7(c) is the depth uncertainty induced by the combined effect of baseline decorrelation (intrinsic), additive noise, and the signal duration, and hence is a more comprehensive representation of the depth uncertainty due to the errors in the detection instant for the different pulse types. It is seen that for the CW pulse with the shortest duration, the additive noise deteriorates the bathymetric uncertainty for the outer beams (this deterioration was also observed in the estimate of the phase difference, see Fig. 6). Regarding the CW pulse with the longest duration and the

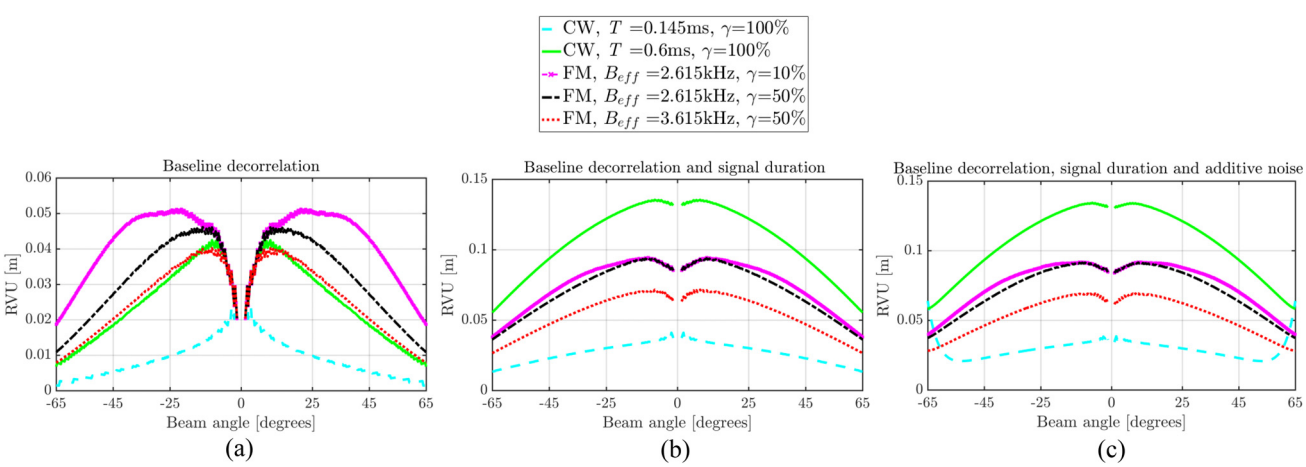

FIG. 7. (Color online) Predicted bathymetric uncertainty due to the (a) baseline decorrelation, (b) baseline decorrelation and signal duration, and (c) baseline decorrelation, signal duration and additive noise for CW and FM pulses with different specifics.

three FM pulse shapes, no noticeable difference was observed compared to Fig. 7(b) (where only the uncertainty induced by the baseline decorrelation and signal duration were considered).

As mentioned, the backscatter strength is related to seabed characteristics such as sediment bulk density, seafloor roughness, volume heterogeneity, and discrete scatterers[41] and the SNR (and consequently the additive noise) is thus different for varying sediment types. To obtain a better understanding of this effect on the additive noise, two sediment types, i.e., clay and sandy gravel, representative of fine and coarse sediments are considered. The depth uncertainty induced by the combined effect of the baseline decorrelation, signal duration and additive noise for the CW pulse with the duration of 0.145 ms (light color) and the FM pulse with the effective bandwidth of 2.615 kHz and 10% tapering value (dark color) considering these two sediments are shown in Fig. 8. To highlight the effect of additive noise, the level of transmitted power is assumed to be 20 dB lower than the maximum power available at the transmission. It is seen that for the fine sediment (clay) shown with solid curve, the additive noise deteriorates the RVU to a larger extent than that of the coarse sediment (sandy gravel) shown with dashed curve which is due to the higher SNR of the former resulting from the higher backscatter values.[34,42]

IV. AN ASSESSMENT OF THE RELATIVE CONTRIBUTION OF THE EFFECTS OF DOPPLER AND BASELINE DECORRELATION

In this section the bathymetric uncertainties induced by the baseline decorrelation and uncertainties in the Doppler effect are compared to the total depth uncertainty predicted. For the prediction of the total bathymetric uncertainty, use is made of Refs. 19 and 20 considering only the contributors relative to the MBES transducer (see the Appendix for the description of the equations used). The uncertainty

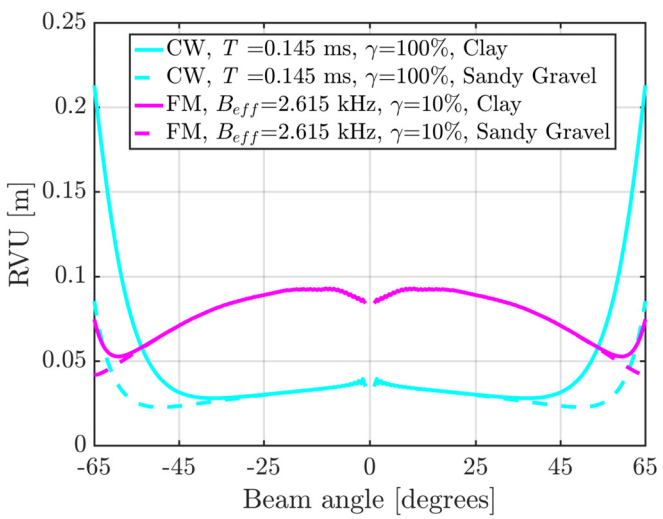

FIG. 8. (Color online) Predicted bathymetric uncertainty due to the baseline decorrelation, signal duration and additive noise for CW with the pulse length of 0.145 ms [light (cyan)] and FM with the effective bandwidth of 2.615 kHz and 10% tapering value [dark (magenta)] pulses for clay (solid) and sandy gravel (dashed).

prediction model was developed under the assumption of independent contributors and flat seafloor. Modelling the uncertainties for a non-flat seafloor requires information regarding the bottom prior to the data acquisition, which is not always feasible. Therefore, we have used model of in Refs. 19 and 20. Using Eqs. (A1)–(A6) (see the Appendix), the errors due to range measurement, roll and steering angles, pitch angle, along track opening angle, sound speed profile, and the resulting total RVU (TRVU) are calculated. It should be noted that for the calculation of TRVU, the contribution of the Doppler effect has not been considered. This enables us to investigate the magnitude of the underestimation of the depth uncertainty that occurs in case of not accounting for the Doppler induced error.

Presented in Fig. 9 is the predicted bathymetry uncertainty due to the total and individual error sources (68% confidence level) for the CW pulse with the duration of 0.145 ms and FM pulse with the effective bandwidth of 2.615 kHz. For the errors related to the range measurements, the sum of the contribution of the baseline decorrelation, signal duration and uncertainty in the measurements of the average sound speed, Eq. (A1), is considered.

The characteristics of the EM2040c (Table II) were used as the input parameters to predict the uncertainty in the bathymetry measurement for a given depth (60 m) as shown in Fig. 9. In addition to the characteristics of the MBES, the characteristics of the sound speed measurements and the motion sensor are also of great importance. Phins[43] was used as the inertial navigation sensor for providing position, true heading, attitude, speed, and heave. The roll and pitch accuracies of the system are 0.01° (the misalignment accuracies are assumed to be 0.02°).[43] The sound velocity profiler is a miniSVP manufactured by Valeport. The accuracy of the system indicated by the manufacturer is 0.02 m/s.[44] However, from measurements in different locations (inland waterways and the North Sea), the uncertainty was found to be 0.2 m/s, and hence this value is chosen as a more realistic description of the system's accuracy. A constant sound speed of 1500 m/s in the water column and 1505 m/s at the transducer are assumed. It should be highlighted that the uncertainty predictions presented in Fig. 9 are based on the specifications discussed above and illustrated in Table II and are not to be viewed as the uncertainty predictions applicable to a different scenario.

For the FM pulse, the contribution of the errors in the range measurements (grey cross markers), i.e., baseline decorrelation and the signal duration, is higher than that of CW which is due to its longer effective pulse length. The additive noise consideration does not affect the depth uncertainty for the FM pulses with the specifics considered here; the error due to the range measurements with and without additive noise coincide. However, for the CW pulse with the duration of 0.145 ms, if the contribution of the additive noise is considered, the range measurements errors (solid grey curve with cross markers) increase for +/−55° beam angles onward, see Fig. 9(a), exceeding that of the considered FM for the outer most beams. As mentioned, regarding the contribution of other sources of uncertainty as derived by

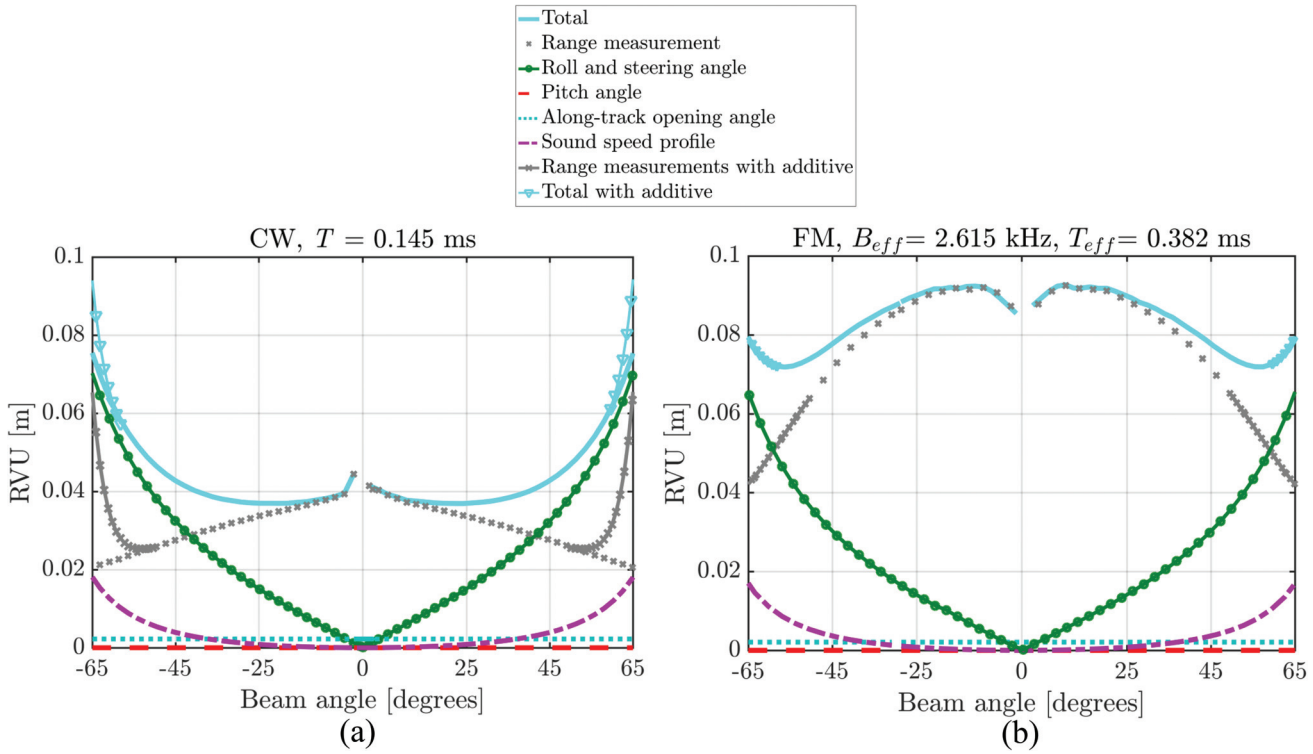

FIG. 9. Predicted uncertainties in the bathymetric measurements. Here, the contribution of heave, dynamic draft, and tidal corrections are not considered, (a) CW with the pulse length of 0.145 ms and (b) FM with the effective pulse length of 0.382 ms.

Refs. 19 and 20, no distinction is made between CW and FM pulses.

As can be seen from Fig. 9, the maximum TRVU without considering the additive noise (solid cyan curve) is nearly 0.08 m for both pulse types. While the TRVU for the outer most beams is nearly equal for CW and FM pulses, for the inner beam it is larger for the FM pulse due to the larger uncertainty in the range measurements making it a dominant contributor to the TRVU. Again, if the additive noise is considered for the CW pulse, the maximum TRVU (solid cyan curve with downward pointing triangle markers) will increase for the outer beams (the central sector is not affected by additive noise as the baseline decorrelation is the dominant source of uncertainty for these beams) and for the outer most beams the TRVU would be slightly larger than that of FM.

With regards to the errors induced by the Doppler in case of using FM (with an effective bandwidth of 2.615 kHz) and CW pulses (with the duration of 0.145 ms) in a rough weather condition [dashed (for CW) and solid (for FM) curves in Figs. 4(a) and 4(b), respectively], one can expect uncertainties of around 0.065 m at $+/-65°$, respectively. Comparing the TRVU to those induced by Doppler when using FM and CW, the maximum Doppler impact is nearly 82% of the total error budget. Hence, it is important to consider the uncertainty induced by the former to obtain a realistic description of the bathymetry uncertainty. With regards to the calm sea state, the contributions are 68% of the total TRVU.

As mentioned, for the calculation of the errors due to the range measurements we have used the uncertainties induced by the baseline decorrelation in the interferometry step, see Eq. (19), where $\sigma^2_{\Delta\phi}$ is due to the baseline decorrelation. However, in Ref. 20 a different approach was taken which was discussed in Sec. II, see Eq. (14). It has been shown that these two approaches are in agreement, see Eqs. (19) and (20) except for a coefficient Q equaling $\sigma_{\Delta\phi}/(2\pi\cos\theta)$ and $0.2/3$, respectively. Shown in Fig. 10 is the value Q for both expressions. For the CW pulse with the shortest duration, the

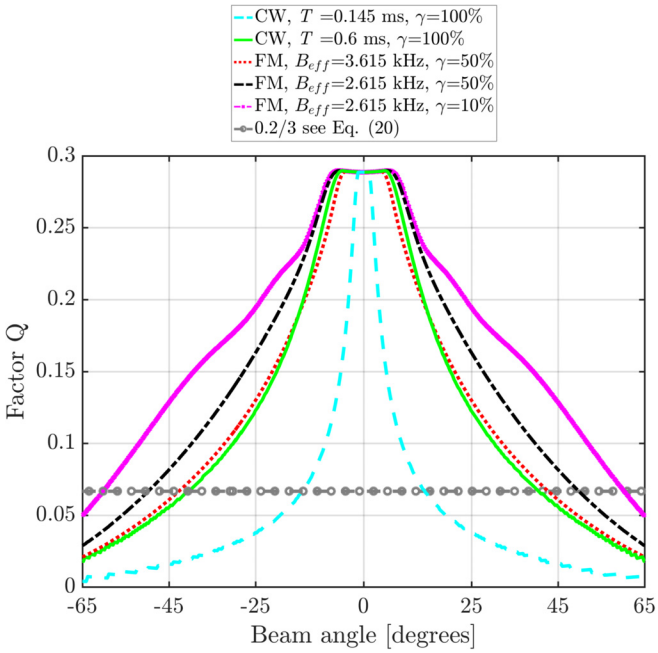

FIG. 10. (Color online) Estimated factor Q used for predicting the baseline decorrelation for FM and CW pulses with different specifics and the factor Q as in Ref. 20.

factor based on the baseline decorrelation is larger than that of Ref. 20 for beam angles up to +/−15°, and hence using the latter leads to an underestimation of the uncertainties. However, as the duration of CW pulse increases, the baseline decorrelation increases and the underestimation occurs for a broader range of inner beams in case of using Eq. (20). With regards to the FM pulse shapes with nearly a rectangular shape (lowest smoothing), the factor Q based on baseline decorrelation is larger than the one based on Ref. 20 for almost the complete swath. However, transmitting a smoother signal and widening the effective bandwidth, decreases the range where the underestimation of the uncertainties occur.

V. ANALYSIS OF MBES EXPERIMENTAL DATA IN CW AND FM MODES

To assess the agreement between the modelled and measured uncertainties, a survey was carried out on 17th of August 2017 in the Westerschelde Estuary connecting the Scheldt River to the North Sea.

The data were acquired using the EM2040c dual head in both CW and FM modes with a center frequency of 300 kHz and pulse lengths of 0.145 and 3 ms (effective bandwidth of 2.615 kHz), respectively. The sea state during the measurement was rough. The bathymetry within the area varies between 46 and 71 m and is shown in Fig. 11. The equiangular beam spacing with the normal detector mode was used. Filters and gains available in EM2040c were turned off. For a detailed description of the filters available and Kongsberg recommendations, one can refer to Refs. 45 and 46.

From Secs. II–IV we do expect equal depth uncertainty for both CW and FM induced by the Doppler effect due to the beamsteering. However, when the FM pulse is used an additional error due to the imperfectness of the Doppler-range correction occurs. With regards to the uncertainties induced by the baseline decorrelation and signal duration [see Figs. 7(a) and 7(b)], it can be concluded that for the CW pulse used during the survey, the uncertainties due to the abovementioned sources are smaller than those of the FM with either of the tapering values (as the exact tapering value is not known) and bandwidths. Regarding the uncertainties induced by the baseline decorrelation, additive noise and signal duration, see Fig. 7(c), it can be concluded that for the CW pulse used during the survey the uncertainties due to this source can get larger than those of FM for the outer beams. In addition to the abovementioned uncertainty sources, one might suspect that another contributor to the deterioration of the quality of the bathymetric measurements in the FM mode is the loss of dual swath capability due to the duty-cycle limitations.[47] However, the pulse length was not so long that the duty-cycle of the transmitter is exceeded and hence this is not a contributing issue.

Shown in Fig. 12 is the standard deviation of the depth measurements for four different areas indicated by the black rectangles in Fig. 11 as **A** [(a) and (b)], **B** [(c) and (d)], **C** [(e) and (f)], and **D** [(g) and (h)]. These results are derived based on a grid with a cell size of 0.5 m × 0.5 m and each

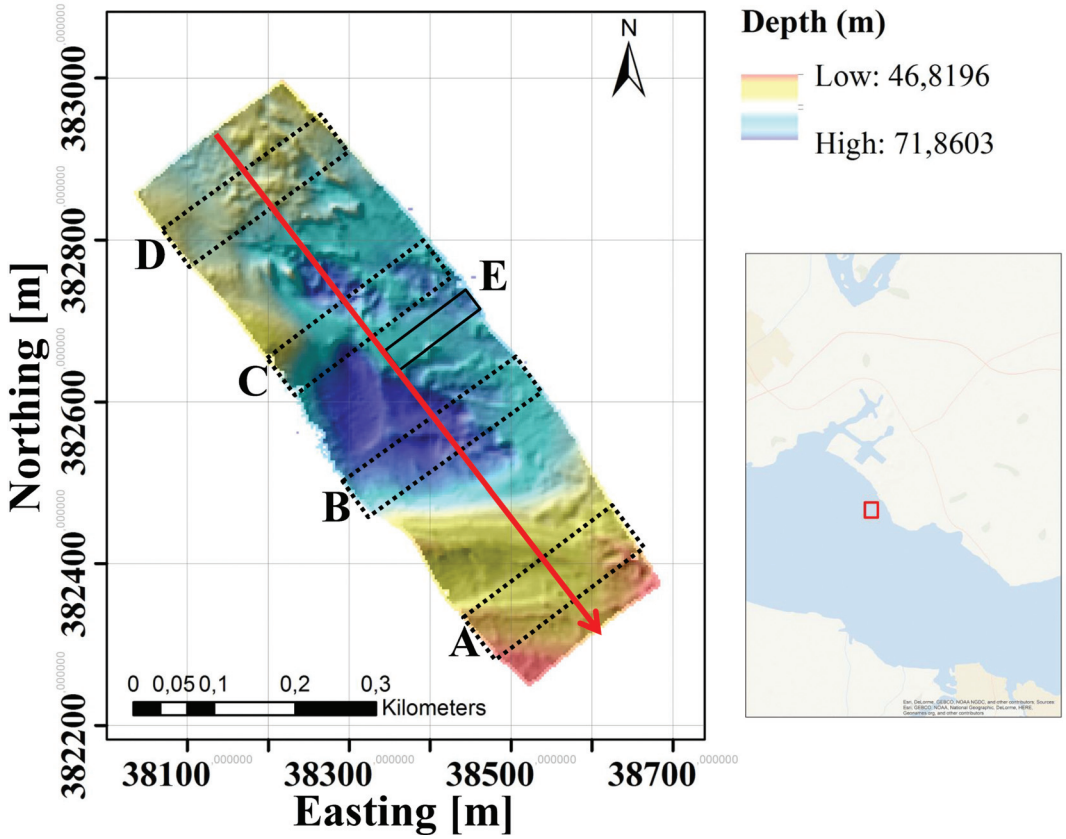

FIG. 11. Bathymetry map of the survey area in the Westerschelde Estuary. The black dashed and solid rectangles indicate the areas used for later plots. The red arrow shows the sailing direction.

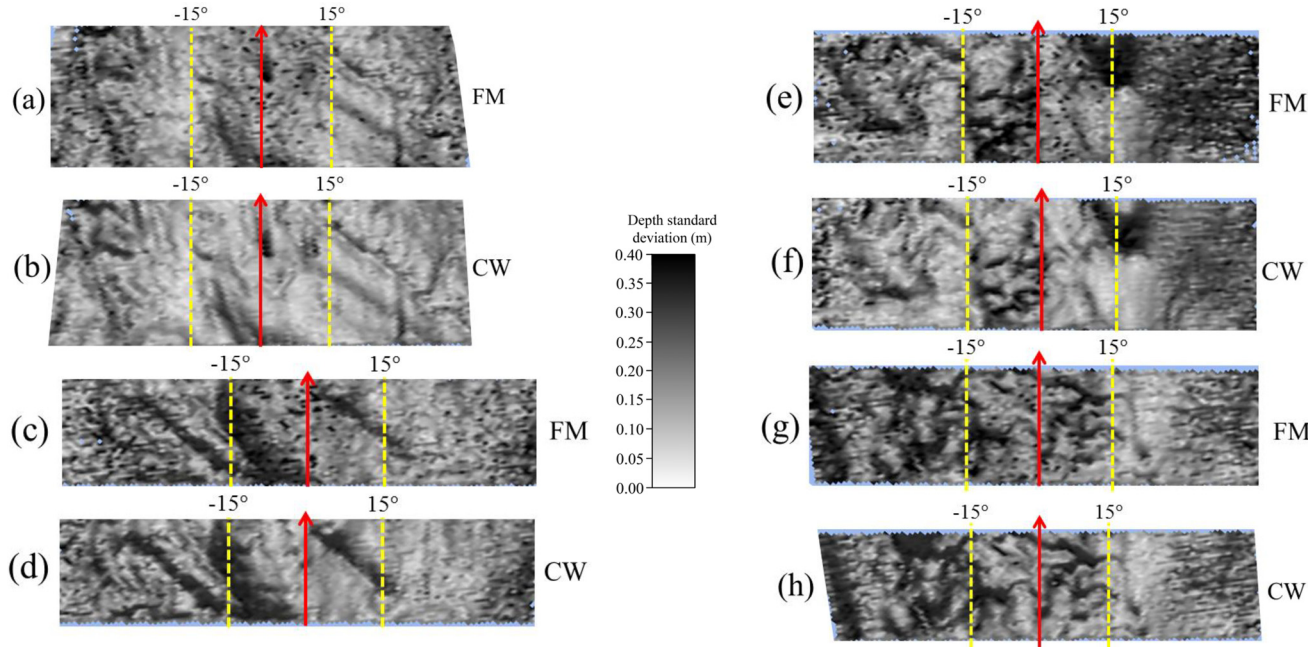

FIG. 12. (Color online) Standard deviation of the depth measurement for the areas shown with the dashed rectangles in Fig. 11 in case of using FM and CW pulses, (a) area **A** with FM, (b) area **A** with CW, (c) area **B** with FM, (d) area **B** with CW, (e) area **C** with FM, (f) area **C** with CW, (g) area **D** with FM, (h) area **D** with CW. This figure is produced using QIMERA processing software [developed by Quality Positioning Service (QPS) BV]. The red arrows show the sailing direction. The dashed yellow shows the $+/-15^\circ$ beam angles.

pixel value is the standard deviation obtained from the depth measurements located in a cell. As the pixel gets darker, the standard deviation increases. While Figs. 12(a), 12(c), 12(e), and 12(g) represent the situation for FM, Figs. 12(b), 12(d), 12(f), and 12(h), illustrate the surfaces derived from the measurements using CW. These figures are composed from separate sets of measurements, i.e., one track uses one pulse type only and the sailing direction was the same for both pulse types. It is seen that the measurements in the FM mode are in general noisier than their CW counterparts. It is also seen from all frames of Fig. 12 that the standard deviation in each cell strongly correlates with the seabed morphology, see the larger standard deviation for non-flat bottoms.

It has been mentioned earlier that in this contribution the seafloor is assumed to be flat. Thus, to have a fair comparison between the predicted (from the model) and real (from the depth measurements) bathymetric uncertainties, flat parts of the surveyed area are chosen. Within the surveyed area, the region satisfying this condition to some extent is the starboard of the black rectangle indicated as **B** in Fig. 11 corresponding to Figs. 12(c) and 12(d). As the port side exhibits significantly larger standard deviation compared to the starboard due to the presence of the morphological features, it has been excluded from the comparison. Still, also for the starboard, the bottom is not completely flat. Another area considered for the comparison of the predicted and measured uncertainties is the solid rectangle indicated by **E** in Fig. 11 (corresponding to the port sides) which is relatively flat. Areas **B** and **E** contain 110 and 50 pings, respectively, which is sufficient to provide a reliable estimate of the standard deviation.

As the first step, the variation of the measured speeds at transmission is considered. The speeds in the easting, northing, and down direction are stored in the Network Attitude datagram and they are projected on the beam direction using the motion and position sensor outputs. Shown in Fig. 13 is the variation of the speeds over the surveyed area for different beam angles. Also indicated, for illustration purposes, is the speed used for the model predictions in the Secs. III–IV. The difference for FM and CW is due to slightly different sea state conditions and ship attitudes over the two tracks. As for the uncertainties of the speed estimates, the maximum allowable uncertainties indicated by Kongsberg for this value is 0.03 m/s in all directions, i.e., easting, northing, and downward.[36] However, this is seen to be lower than the uncertainties from Fig. 3(b). Still Fig. 3(b) was derived using the uncertainties of the equipment that was used for the August 2017 survey and thus are considered to represent the real uncertainties.

To calculate the Doppler effect on beamsteering (existing for both CW and FM pulses) and matched filtering (only for FM pulses), a bin size of 2° is considered and the average beam angle and depth of the soundings per bin, along with the measured variation and uncertainties of the speeds are used in Eqs. (12) and (13). Shown in Figs. 14(a) and 14(b) are the predicted depth uncertainties induced due to the use of CW and FM pulses for the starboard of the area indicated by **B** in Fig. 11, respectively.

Comparing Fig. 14(a) with Fig. 4(a), slightly higher uncertainties are found now as expected from Fig. 13. Shown with the light dashed gray in Fig. 14(b) are the uncertainties due to the matched filtering step in case the Kongsberg specifications are used, indicating that in practice uncertainties due to the Doppler in matched filtering are twice as high. A similar situation also holds for the area **E** in Fig. 11.

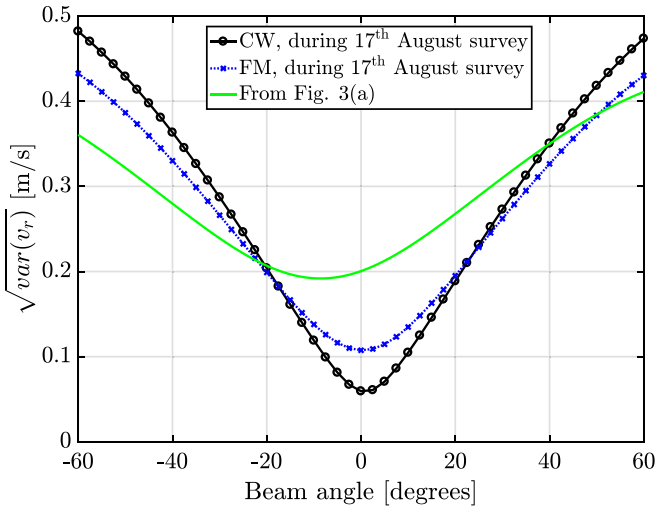

FIG. 13. (Color online) square root of the speeds variations.

The other source of uncertainty affecting the quality of MBES bathymetric measurements differently when using CW and FM pulses, is the baseline decorrelation, see the developed model and its quantification for the operational environment in Secs. III and IV, respectively. It should be noted that, as discussed, except for the errors due to the baseline decorrelation, the second-order Doppler effect (imperfectness of Doppler correction), and signal duration, the contribution of the other error sources to the depth measurements uncertainties are assumed to be equal for both pulse shapes. Therefore, to eliminate the effect of these types of contributors, from this point onward, the difference between the CW and FM pulses are considered, i.e., the effect of switching from CW to FM pulse is analyzed. Ideally, for the analysis of the effect of switching from CW to FM pulse, the data in both modes have to be acquired simultaneously. If the time interval between the data acquisition in the two modes amounts to several days, the difference between the depth measurements (or other indicators) using CW and FM pulses is not solely affected by the pulse type as the bottom features can vary due to sediment transport. However, for the data set analyzed here, the time interval between measuring the two track lines with varying pulse type was around 45 min. The features such as ripples and sand waves are thus not expected to vary significantly within this period, i.e., sediment transport does not occur to a significant extent. Still, a small effect might be observed due to this phenomenon.

To assess the performance of the model developed for quantifying the effect of baseline decorrelation, use is made of the quality factor stored in the datagrams during the data acquisition. The quality factor, stored in the raw range and angle datagram (datagram 78), is defined in Ref. 8 as the standard deviation of the range divided by the detected range. The parameters affecting this standard deviation are thus the signal noise at the detection instant and the uncertainty in the estimate of the zero-crossing using the linear fit to the measurements of the phase difference. Shown in Figs. 15(a) and 15(b) with circles is the measured difference between the standard deviation of the detected range projected on the depth axis for the FM and CW pulses derived from the quality factor for the phase detection for areas **E** and **B** in Fig. 11. Shown with the solid curve is the modeled difference between the standard deviation of the detected range induced by the baseline decorrelation for FM and CW pulses, see Eq. (19) and Fig. 7(a). For beam angles larger than $+/-15°$, the behavior of the modelled differences follows those measured. For beam angles close to the nadir, the interferometry, ill-adapted to too short time signals is replaced by the amplitude detection, which is the detection of the echo arrival time based on the analysis of signal envelope.[28] The effect of different pulse shapes on the amplitude detection is not considered here.

As a final step, the comparison between the modelled and measured differences between the standard deviation of the final depth measurements using FM and CW pulses is carried out. Again, a bin size of 2° is considered and the

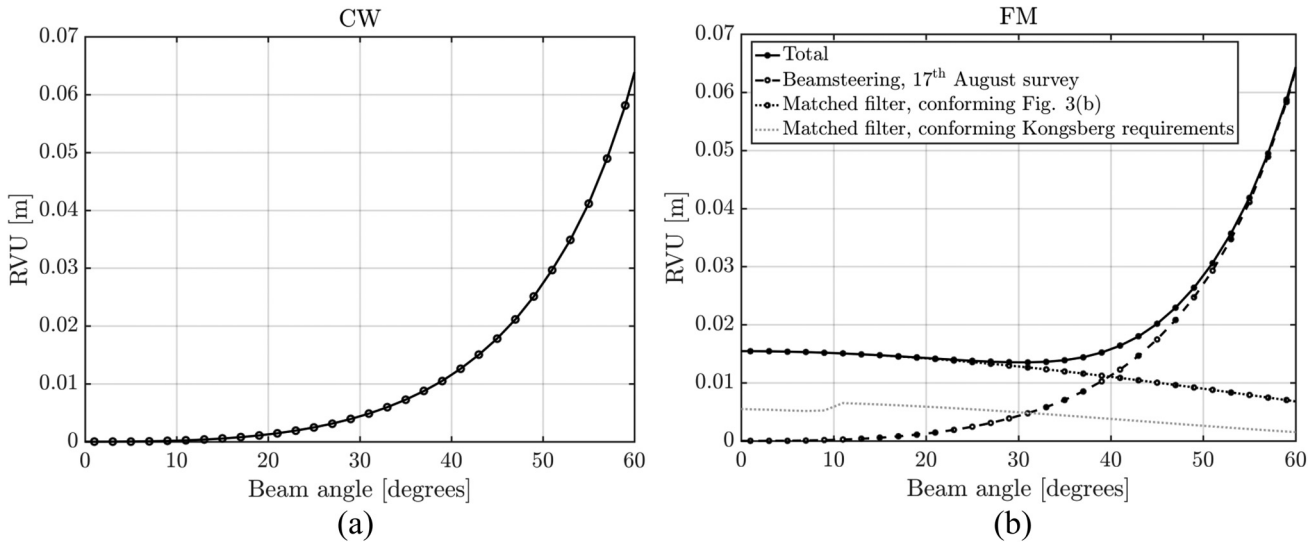

FIG. 14. (a) Bathymetric uncertainty due to the Doppler effect for the CW pulse and (b) bathymetric uncertainty due to the Doppler frequency shift for the FM pulse (with circles) and bathymetric uncertainty due to Dopplerized matched filter for the FM pulse according to the Kongsberg requirements (dotted light) for the starboard of the area **B** in Fig. 11.

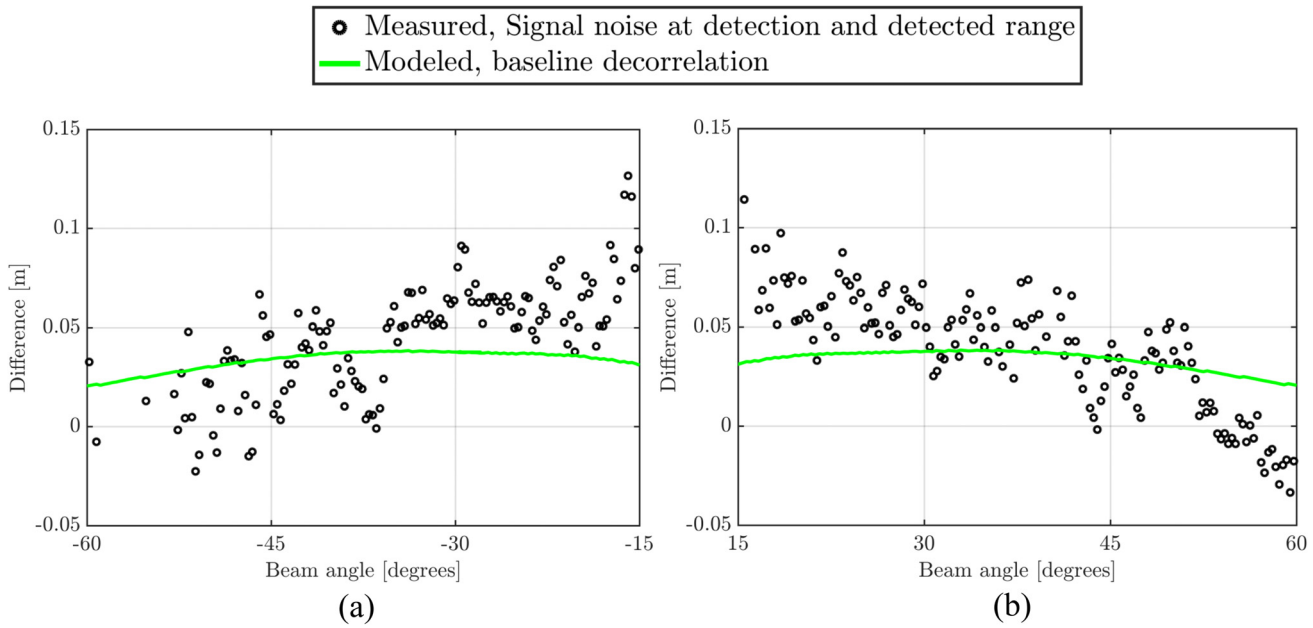

FIG. 15. (Color online) Modeled (solid curve) and measured (circles) difference between the uncertainty of the detected range projected on the depth axis using FM and CW pulses for (a) area **E** and (b) area **B** in Fig. 11.

variations of the depth measurements for different bins are considered. Shown with the solid curve with circles in Figs. 16(a) and 16(b) is the difference between the standard deviation of the depth measurements using FM and CW, where the positive values indicate a higher standard deviation for the FM than that of CW, for areas **E** and **B**, respectively. Shown with the solid curve with crosses is the predicted difference accounting for all aspects addressed in Secs. II–IV. For illustration purposes, the curves without accounting for signal duration and/or additive noise are also shown.

This indicates that including the contribution of the signal duration affects the beams close to the nadir the most. The comparison between the full model and measured curves indicates a relatively good agreement for areas **E** and **B** in Fig. 11. The agreement between the modeled and measured differences indicates that accounting for the depth uncertainty due to the errors in the Doppler range correction and the combined effect of the baseline decorrelation and the signal duration can capture the difference observed in the vertical uncertainty when switching from CW to FM for a flat seafloor. The discrepancies between the model and the measured differences are associated to the bottom morphology. It can also be seen that the effect of additive noise on the differences is almost negligible for the beam angles considered here.

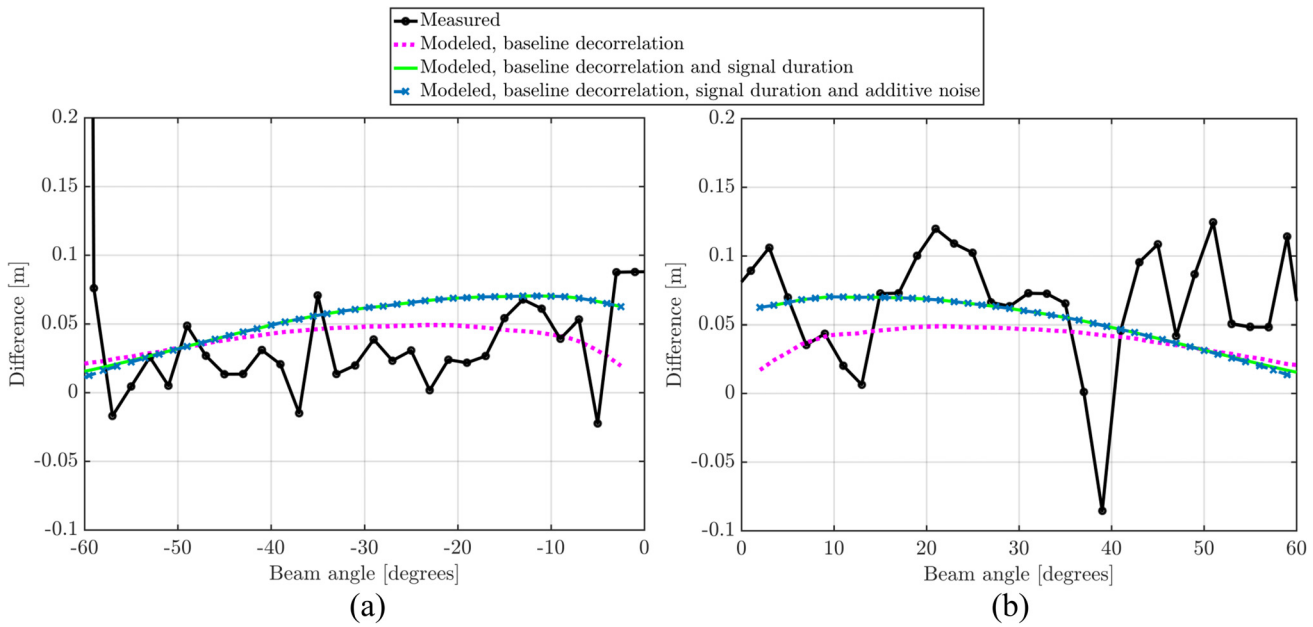

FIG. 16. (Color online) difference between the standard deviation of depth measurements using FM and CW pulses as measured (solid curve with circle markers) and modelled using baseline decorrelation (dotted) plus the signal duration (solid curve) plus the additive noise (dashed curve with cross markers), i.e., $\sigma_{\mathrm{FM}-}\sigma_{\mathrm{CW}}$, for (a) area **E** and (b) area **B** in Fig. 11.

VI. CONCLUSIONS

New generation MBES systems are able to transmit both FM and CW pulse shapes, whereas in the past the only pulse used was CW. FM pulses allow for measurements at larger ranges resulting in an increase in the attainable swath. However, in contrast to the expectations, in some cases the performance of the bathymetry measurements was reported to deteriorate when switching from CW to FM. Two origins have been identified for the increase in the depth variations when using FM: the Doppler frequency shift due to the motion of the MBES sensor and baseline decorrelation. In this contribution, depth uncertainties induced by both effects were quantified for the EM2040c dual head in a shallow water environment (water depth of around 60 m) and rough and calm sea states. The contribution of the Doppler effect was compared to the depth uncertainty induced by the combination of the errors in the range measurements [due to the baseline decorrelation and the signal duration (and additive noise)], roll and steering angle, pitch angle, along track opening angle, and sound speed profile, which are the contributors relevant to the depths relative to the MBES transducer. Measurements acquired in the FM and CW modes using EM2040c dual head were analyzed to validate the uncertainty prediction model.

Based on the results of the modelling and real measurements, the following conclusions can be drawn:

- The bathymetric uncertainty induced by the Doppler effect in the beamsteering process is equal for both pulse types and as it is not corrected for by the manufacturer, its contribution is a first-order effect. For the rough sea state, the vertical uncertainty induced by this source can be up to 82% of the total TRVU (for the calm condition the contribution is 80% of the rough sea state). To take the contribution of this error source into account in the bathymetry uncertainty model, an additional term should be added to the equation describing the random depth error due to the uncertainty in the roll and steering angle.
- The bathymetric uncertainty resulting from the imperfectness of the correction applied to counteract the Doppler frequency shift occurs only for the FM signal and thus its associated uncertainty is a second-order effect. Its contribution to the TRVU is much smaller than the contribution of the Doppler effect on the steering angle. In order to consider its contribution, the term defining the random depth error due to the error in the measured distance should be modified.
- Taking these error sources into account in the uncertainty prediction model allows one to have a more realistic description of the bathymetry uncertainty. These terms do, however, require knowledge on the transducer motion and are sea state dependent.
- The baseline decorrelation induces an uncertainty in the estimation of the phase difference leading to an uncertainty in the derived depth. For the FM and CW pulse specifications considered in this contribution, the depth uncertainty for the former is larger than that of the latter (except for the FM pulse with effective bandwidth and tapering values of 3.615 kHz and 50%, respectively). However, this does not mean that the depth uncertainty is higher for FM than that of CW irrespective of the pulse shape. For the CW pulse, the bathymetric uncertainty due to the baseline decorrelation decreases with shortening pulse length. Widening the bandwidth and increasing the tapering coefficient of the FM pulse (reduction of the sidelobes) also lead to a decrease in the depth uncertainty induced by this error source.
- Although using a shorter CW pulse improves the coherence between the two received signals leading to a decrease in the uncertainty induced by the baseline decorrelation, it also reduces the received acoustic energy. Hence, the SNR deteriorates. The SNR has been simulated for a flat muddy sand bottom assuming a maximum transmitted energy level of the MBES. It was found that for the CW pulse with the shortest duration, the worsening of the SNR dominates the depth uncertainty for the outer beam sector (larger than $+/-55^{\circ}$) and the final bathymetric uncertainty for this pulse type can be larger than those of FM for these beams. The exact behavior is dependent on the sediment type and source level.
- Finally, measurements indicate that indeed the use of FM pulses can result in a noisier bathymetry. To assess the agreement between the measured and modelled uncertainty, two relatively flat areas consisting of a number of pings have been chosen. Good agreement is found between the measured and predicted effect of switching from CW to FM pulses.

ACKNOWLEDGMENTS

We would like to thank Simon Bicknese and Ben Dierikx from the Dutch Ministry of Infrastructure and the Environment for their support in this research and their very valuable input.

APPENDIX: MODELLING THE BATHYMETRIC UNCERTAINTY DUE TO THE SOURCES INHERENT TO THE MBES

In Sec. II, the uncertainty in the MBES bathymetric measurements due to Doppler and baseline decorrelation was assessed. However, there are more sources of uncertainty. For investigating the importance of the Sec. II sources of uncertainty, they need to be compared to the total uncertainty.

MBES surveys are carried out for, for example, identifying seabed typologies,[48,49] monitoring the marine environment to guarantee safe navigation, and habitat mapping.[50] Bathymetric features, such as depth residuals,[51,52] have also found their way to sediment classification. All these applications require knowledge about the uncertainties of the bathymetric measurements. Consequently, predicting the uncertainty in MBES bathymetric measurements is nowadays an important and almost standard step in the planning of MBES surveys and models for predicting this uncertainty have been developed. The reason for this is that they enable one to assess whether the required survey standards can be met in a specific measurement campaign. In recent years,

predicting bathymetric uncertainty has become a common practice. Reference 53 looked at the uncertainty estimation in legacy data sets and errors induced by different gridding methods. In Ref. 54 the archival data are compared to the modern MBES data in shallow water (35–110 m depth) from the uncertainty point of view. Reference 55 developed a model for the error budget by comparing single beam echo sounder (SBES) and MBES data in deep water. Reference 56 developed a bathymetric uncertainty model for L-3 Klein 5410 phase differencing sonar based on the approach presented by Refs. 19 and 20. In this contribution the focus is also on the depth uncertainty model derived in these references in which the total propagated uncertainty is determined using the assumption of independent uncertainty contributors. In this Appendix, a brief overview of the model is given.

Assuming non-zero roll (R) and pitch angles (P), see Fig. 17, the depth (d) is determined from Eq. (11), i.e.,

$$d = r\cos P\cos(\theta_s + R + \theta_{\text{mount}}) = r\cos P\cos\theta.$$

Based on this expression, the following contributions to the total uncertainty in the calculated depths are identified in Ref. 19.

1. Range measurement ($\sigma^2_{d_1}$)

Since the travel time of the signal and the speed of sound are used to determine the range under a certain beam angle (r, see Fig. 17) the uncertainty in the measurement of these parameters introduces uncertainties in the range measurement and consequently the depth. The expression for the uncertainty of the travel time in case of phase detection was already discussed in Sec. II. It should be noted that there the uncertainty in the detection instant ($\sigma^2_{t_D}$) was considered as a combination of uncertainty due to the baseline decorrelation and the signal duration. Thus, the resulting expression for the depth uncertainty due to the range measurements becomes

$$\sigma^2_{d_1} = \left(\frac{c}{2}\cos P\cos\theta\right)^2\left(\sigma^2_{t_D} + \left(\frac{2r_{\text{meas}}}{c}\right)^2\sigma^2_c\right), \tag{A1}$$

where r_{meas} is the measured distance and σ^2_c is the uncertainty in the sound speed (average over water column).

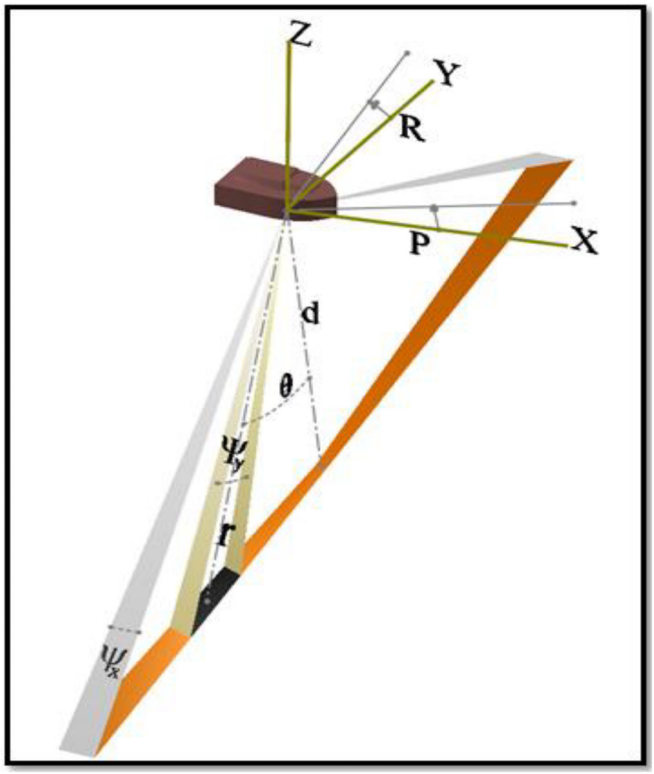

FIG. 17. (Color online) Schematic of the MBES swath and orientation of the vessel, showing parameters relevant for estimating the random depth uncertainty.

2. Roll and steering angle ($\sigma^2_{d_2}$)

Uncertainty in the beam steering angle due to fluctuations in the sound speed at the transducer ($\sigma^2_{c,s}$), roll measurements ($\sigma^2_{R_{\text{meas}}}$), and roll alignment ($\sigma^2_{\Delta R_{\text{align}}}$) of the MBES transducer results in the uncertainty in the angle of impact of the sound on the MBES and consequently the depth measurements which is of the following form:

$$\sigma^2_{d_2} = (r\cos P\sin\theta)^2(\sigma^2_{c,s} + \sigma^2_{R_{\text{meas}}} + \sigma^2_{\Delta R_{\text{align}}}), \tag{A2}$$

where $\sigma^2_{c,s}$ follows from Ref. 19. If roll correction is applied during beamforming, additional uncertainties emerge due to imperfectness of this correction and conform[20] a second pair of roll errors, $\sigma^2_{R_{\text{meas}}} + \sigma^2_{\Delta R_{\text{align}}}$, is added.

3. Pitch angle ($\sigma^2_{d_3}$)

Errors in the pitch measurements ($\sigma^2_{P_{\text{meas}}}$) and pitch alignment ($\sigma^2_{\Delta P_{\text{align}}}$) affect the angle in the along-track direction and thus contribute to the depth error. The expression for this uncertainty is

$$\sigma^2_{d_3} = (r\cos\theta\sin P)^2(\sigma^2_{P_{\text{meas}}} + \sigma^2_{\Delta P_{\text{align}}}). \tag{A3}$$

Similarly, if a pitch correction is applied during beamforming, a second pair of errors, $\sigma^2_{P_{\text{meas}}} + \sigma^2_{\Delta P_{\text{align}}}$, is added.

4. Along-track opening angle ($\sigma^2_{d_4}$)

The non-zero beam along-track beam opening angle, ψ_x, limits the depth resolution, resulting in an error in the depth calculation in case of a non-flat seafloor. The contribution of this error source to the random depth error is modeled as

$$\sigma^2_{d_4} = d^2\left(1 - \cos\frac{\psi_x}{2}\right)^2. \tag{A4}$$

5. Sound speed profile ($\sigma^2_{d_5}$)

The non-uniform sound speed profile (SSP) through the water column results in the deviation of the sound rays from straight lines. The calculated position and depth thus differ from the true position and depth. If the sound speed in the water column differs from the measured one, then the

bathymetry shows "smiley" or "droopy" effects.[57] The SSP correction carried out in the post-processing mode is particularly important in highly dynamic environments, such as the Rotterdam Waterway where the Meuse River meets the North Sea and the varying presence of salt and fresh water results in a large variation in SSP. For the data sets considered in this contribution, this was not the case. With regards to the sound speed error consideration in the error budget prediction for the survey planning, different approaches are available. Reference 58 developed a simulation tool which enables the assessment of the impact of water column variability on depth uncertainty. The method is based on mimicking the ray tracing portion of the depth reduction procedure and gives an estimation of the depth bias in case an erroneous sound speed profile is used. Another approach, presented by Ref. 19, is based on the two layer sound speed profile. Assuming an equal thickness for both layers, an approximation for the error in the beam angle induced by the error in the sound speed profile is obtained. This method does not require ray tracing, and hence is faster compared to the simulation tool. It might, however, lead to an underestimation of the uncertainty and is known to be limited by the assumption of the two-layer SSP. Still, in the present contribution we adopted this approach. The contribution of this error term, assuming the two-layer representation of the sound speed profile, is

$$\sigma_{d_5}^2 = (r \cos P \sin\theta)^2 \left(\frac{\tan\theta}{2c}\right)^2 \sigma_c^2. \tag{A5}$$

Furthermore, an uncertainty with regards to the vessel heave (combination of the measurement error of heave and the induced heave) and variation in the water level induce an error in the depth estimation. The uncertainty due to the former depends on the relative location of the MBES transducer and the vertical reference unit and does not solely depend on the MBES in contrast to those discussed above, see Eqs. (A1)–(A5). The uncertainty due to the variations in the water level and that of the GPS also do not depend on the MBES. As the focus here is on the contributors relevant to the depths relative to the MBES transducer, these sources have been excluded from the calculation of the TRVU. For a detailed description of all error sources and derivation of the above equations, one may refer to Refs. 19 and 20.

The TRVU is determined as the sum of above error sources as

$$\sigma_d^2 = \sigma_{d_1}^2 + \sigma_{d_2}^2 + \sigma_{d_3}^2 + \sigma_{d_4}^2 + \sigma_{d_5}^2. \tag{A6}$$

Here, it is assumed that these error sources are independent from each other. An interested reader might refer to Ref. 56 for the expressions related to the covariance considerations. Environmental aspects such as a non-flat seafloor and variation in sediment characteristics will add to the uncertainty of the bathymetric measurements.

[1]J. R. Klauder, A. C. Price, S. Darlington, and W. J. Albersheim, "The theory and design of chirp radars," Bell. Syst. Tech. J. **39**(4), 745–808 (1960).

[2]J. D. Beaudoin, P. D. Johnson, X. Lurton, and J. M. Augustin, "R/V Falkor multibeam echosounder system review," UNH-CCOM/JHC (2012), Vol. 58, http://mac.unols.org/sites/mac.unols.org/files/20120904_Falkor_EM710_EM302_report.pdf (Last viewed 6/10/2018).

[3]J. D. Beaudoin, P. D. Johnson, and A. F. Flinders, "R/V Falkor multibeam echosounder system review," UNH-CCOM/JHC (2014), Vol. 82, http://mac.unols.org/sites/mac.unols.org/files/20140212_Falkor_EM710_EM302_report_final.pdf (Last viewed 6/10/2018).

[4]P. D. Johnson and K. W. Jerram, "E/V Nautilus EM302 multibeam echosounder system review," CCOM (2014), Vol. 20, https://scholars.unh.edu/cgi/viewcontent.cgi?article=1039&context=ccom (Last viewed 6/14/2018).

[5]P. Vincent, "Modulated signal impact on multibeam echosounder bathymetry," Ph.D. dissertation, Télécom Bretagne Sous En habilitation conjointe avec l'Université de Rennes 1 (2013).

[6]P. Vincent, F. Maussang, X. Lurton, C. Sintes, and R. Garello, "Bathymetry degradation causes for frequency modulated multibeam echo sounders," in *2012 MTS/ IEEE Oceans*, Hampton Roads, VA (2012).

[7]P. Vincent, C. Sintes, F. Maussang, X. Lurton, and R. Garello, "Doppler effect on bathymetry using frequency modulated multibeam echo sounders," in *2011 IEEE—Oceans Spain*, Santander, Spain (2011).

[8]"Instruction manual: EM Series Multibeam Echo Sounder, EM datagram formats," Kongsberg Maritime (2016), https://www.km.kongsberg.com/ks/web/nokbg0397.nsf/AllWeb/253E4C58DB98DDA4C1256D790048373B/$file/160692_em_datagram_formats.pdf?OpenElement (Last viewed 6/18/2018).

[9]Ø. Aasbø, Kongsberg, personal communication (2 August 2017).

[10]C. de Moustier, "State of the art in swath bathymetry survey systems," Int. Hydrogr. Rev. **65**, 25–54 (1988).

[11]J. S. Bird and G. K. Mullins, "Analysis of swath bathymetry sonar accuracy," IEEE J. Oceanic Eng. **30**(2), 372–390 (2005).

[12]G. Llort-Pujol, "Amélioration de la résolution spatiale des sondeurs multifaisceaux (Improvement of the spatial resolution for multibeam echosounders)," Ph.D. dissertation, Télécommunications de Bretagne en Habilitation conjointe avec l'Université de Rennes 1 (2007).

[13]R. O. Nielsen, "Azimuth and elevation angle estimation with a three-dimensional array," IEEE J. Oceanic Eng. **19**(1), 84–86 (1994).

[14]R. O. Nielsen, "Accuracy of angle estimation with monopulse processing using two beams," IEEE Trans. Aerosp. Electron. Syst. **37**(4), 1419–1423 (2001).

[15]C. Sintes, G. Llort-Pujol, and D. Gueriot, "Coherent probabilistic error model for interferometric sidescan sonars," IEEE J. Oceanic Eng. **35**(2), 412–423 (2010).

[16]G. L. Jin and D. J. Tang, "Uncertainties of differential phase estimation associated with interferometric sonars," IEEE J. Oceanic Eng. **21**(1), 53–63 (1996).

[17]X. Lurton, "Swath bathymetry using phase difference: Theoretical analysis of acoustical measurement precision," IEEE J. Oceanic Eng. **25**(3), 351–363 (2000).

[18]X. Lurton, "Theoretical modelling of acoustical measurement accuracy for swath bathymetric sonars," Int. Hydrogr. Rev. **4**(2), 17–30 (2003).

[19]R. Hare, "Depth and Position Error Budgets for Multibeam Echosounding," Int. Hydrogr. Rev. **LXXII**(2), 37–69 (1995).

[20]R. Hare, "Error Budget Analysis for US Naval Oceanographic Office (NAVOCEANO) Hydrographic Survey Systems," Hydrographic Science Research Center (HSRC) (2001), Vol. 155, available at https://www.academia.edu/10086841/Error_Budget_Analysis_For_NAVO?auto=download (Last viewed 6/24/2018).

[21]T. H. Mohammadloo, M. Snellen, and D. G. Simons., "An uncertainty assessment of the effect of using FM pulses on MBES depth measurements," in *4th Underwater Acoustics Conference and Exhibition*, Skiathos, Greece (2017), pp. 1043–1048.

[22]A. W. Rihaczek, *Principles of High-Resolution Radar* (McGraw-Hill, New York, 1969).

[23]L. Bruno, P. Braca, J. Horstmann, and M. Vespe, "Experimental evaluation of the range-Doppler coupling on HF surface wave radars," IEEE Geosci. Remote Sens. Lett. **10**(4), 850–854 (2013).

[24]Y. Pailhas, S. Dugelay, and C. Capus, "Impact of temporal Doppler on synthetic aperture sonar imagery," J. Acoust. Soc. Am. **143**(1), 318–329 (2018).

[25]G. Yufit and E. Maillard, "The influence of ship motion on bathymetric sonar performance in FM mode of operation," in *Oceans 2011*, Waikoloa Village, HI (2011).

[26]J. E. Hughes Clarke, "Dynamic motion residuals in swath sonar data: Ironing out the creases," Int. Hydrogr. Rev. **4**(1), 6–23 (2003).
[27]L. C. Van Rijn, *Principles of Fluid Flow and Surface Waves in Rivers, Estuaries, Seas and Oceans* (Aqua Publication, Amsterdam, 1990).
[28]X. Lurton and J. M. Augustin, "A measurement quality factor for swath bathymetry sounders," IEEE J. Oceanic Eng. **35**(4), 852–862 (2010).
[29]R. J. A. Tough, D. Blacknell, and S. Quegan, "A statistical description of polarimetric and interferometric synthetic-aperture radar data," Proc. R. Soc. London Ser. A **449**(1937), 567–589 (1995).
[30]X. Lurton, *An Introduction to Underwater Acoustics: Principles and Applications*, 2nd ed. (Springer, Berlin, 2010).
[31]D. G. Simons and M. Snellen, "A comparison between modeled and measured high frequency bottom backscattering," in *Proceedings of the European Conference on Underwater Acoustics*, Paris, France (2008), pp. 639–644.
[32]D. D. Sternlicht and C. P. de Moustier, "Time-dependent seafloor acoustic backscatter (10–100 kHz)," J. Acoust. Soc. Am. **114**(5), 2709–2725 (2003).
[33]C. P. de Moustier and H. Matsumoto, "Seafloor acoustic remote sensing with multibeam echosounder and bathymetric sidscan sonar systems," Mar. Geophys. Res. **15**(1), 27–42, https://doi.org/10.1007/BF01204150 (1993).
[34]J. E. Hughes Clarke, L. A. Mayer, and D. E. Wells, "Shallow-water imaging multibeam sonars: A new tool for investigating seafloor processes in the coastal zone and on the continental shelf," Mar. Geophys. Res. **18**(6), 607–629, https://doi.org/10.1007/BF00313877 (1996).
[35]"EM2040C," Kongsberg Maritime (2016), available at https://www.km.kongsberg.com/ks/web/nokbg0397.nsf/AllWeb/38E3552DFEE3BAE3C1257AF5004118FE/$file/369468_EM2040c_product_specification.pdf (Last viewed 6/16/2018).
[36]K. Jensen, Kongsberg, personal communication (30 June 2018).
[37]"Kongsberg EM2040C multibeam echo sounder: Installation manual," Kongsberg Maritime (2015), available at https://www.km.kongsberg.com/ks/web/nokbg0397.nsf/AllWeb/E964407DAB955D02C1258017003C5045/$file/378789-em2040c_installation_manual.pdf?OpenElement (Last viewed 6/22/2018).
[38]APL-UW, "APL-UW high-frequency ocean environmental acoustic models handbook," Applied Physics Laboratory, University of Washington (1994), http://www.dtic.mil/dtic/tr/fulltext/u2/b199453.pdf (Last viewed 6/7/2018).
[39]P. Vincent, F. Maussang, X. Lurton, C. Sintes, and R. Garello, "Multibeam interferometric sounding quality for FM signals: Modelling and comparison with field data," in *2013 MTS/IEEE Oceans—Bergen*, Bergen, Norway (2013).
[40]P. J. G. Teunissen, D. G. Simons, and C. C. J. M. Tiberius, *Probability and Observation Theory: An Introduction* (Delft University of Technology, Faculty of Aerospace Engineering, Delft, the Netherlands, 2006).
[41]D. R. Jackson and M. D. Richardson, *High-Frequency Seafloor Acoustics* (Springer Science, New York, 2007).
[42]C. de Moustier and D. Alexandrou, "Angular dependence of 12-kHz seafloor acoustic backscatter," J. Acoust. Soc. Am. **90**(1), 522–531 (1991).
[43]"Phins: FOG-based high-performance inertial navigation system," iXblue (2017), available at https://www.ixblue.com/sites/default/files/datasheet_file/ixblue-phins-03_2017.pdf (Last viewed 6/25/2018).
[44]"miniSVP-Sound Velocity Profiler," Valeport (2016), http://www.valeport.co.uk/Portals/0/Docs/Datasheets/Valeport-miniSVP.pdf (Last viewed 6/25/2018).
[45]"EM technical note: Filters and gains for EM 2040, EM 710, EM 302 and EM 122," Kongsberg Maritime (2017), https://www.km.kongsberg.com/ks/web/nokbg0397.nsf/AllWeb/0B72C7F9799189ABC1257C7E002E092F/$file/Kongsberg-EM-Technical-Note-EM-Runtime-Parameters-Filters-and-Gains-Basic.pdf?OpenElement (Last viewed 2/10/2018).
[46]"EM technical note: Advanced filters and gains for EM 2040, EM 710, EM 302 and EM 122," Kongsberg Maritime (2017), https://www.km.kongsberg.com/ks/web/nokbg0397.nsf/AllWeb/1ECE817E2D81B2C7C1257C7E002DCF97/$file/Kongsberg-EM-Technical-Note-EM-Runtime-Parameters-Filters-and-Gains-advanced.pdf?OpenElement (Last viewed 2/10/2018).
[47]J. E. Hughes Clarke, "The Impact of acoustic imaging geometry on the fidelity of seabed bathymetric models," Geosciences **8**(4), 109 (2018).
[48]G. Di Maida, A. Tomasello, F. Luzzu, A. Scannavino, M. Pirrotta, C. Orestano, and S. Calvo, "Discriminating between *Posidonia oceanica* meadows and sand substratum using multibeam sonar," ICES J. Mar. Sci. **68**(1), 12–19 (2011).
[49]T. Komatsu, C. Igarashi, K. Tatsukawa, S. Sultana, Y. Matsuoka, and S. Harada, "Use of multi-beam sonar to map seagrass beds in Otsuchi Bay on the Sanriku Coast of Japan," Aquat. Living Resour. **16**(3), 223–230 (2003).
[50]T. J. Anderson, C. Syms, D. A. Roberts, and D. F. Howard, "Multi-scale fish-habitat associations and the use of habitat surrogates to predict the organisation and abundance of deep-water fish assemblages," J. Exp. Mar. Biol. Ecol. **379**(1-2), 34–42 (2009).
[51]D. Eleftherakis, A. Amiri-Simkooei, M. Snellen, and D. G. Simons, "Improving riverbed sediment classification using backscatter and depth residual features of multi-beam echo-sounder systems," J. Acoust. Soc. Am. **131**(5), 3710–3725 (2012).
[52]D. Eleftherakis, M. Snellen, A. Amiri-Simkooei, D. G. Simons, and K. Siemes, "Observations regarding coarse sediment classification based on multi-beam echo-sounder's backscatter strength and depth residuals in Dutch rivers," J. Acoust. Soc. Am. **135**(6), 3305–3315 (2014).
[53]R. Hare, B. Eakins, C. Amante, and L. A. Taylor, "Modeling bathymetric uncertainty," in *U.S. Hydro 2011*, Tampa, FL (2011).
[54]B. Calder, "On the uncertainty of archive hydrographic data sets," IEEE J. Oceanic Eng. **31**(2), 249–265 (2006).
[55]K. M. Marks and W. H. F. Smith, "An uncertainty model for deep ocean single beam and multibeam echo sounder data," Mar. Geophys. Res. **29**(4), 239–250, https://doi.org/10.1007/s11001-008-9060-y (2008).
[56]M. S. Moser, "Bathymetric Uncertainty Model for the L-3 Klein 5410 Sidescan Sonar," M.Sc. thesis, University of New Hampshire, 2009.
[57]D. F. Dinn, B. D. Loncarevic, and G. Costello, "The effect of sound velocity errors on multi-beam sonar depth accuracy," in *Oceans '95 MTS/IEEE—Challenges of Our Changing Global Environment, Conference Proceedings*, San Diego, USA (1995), Vols. 1–3, pp. 1001–1010.
[58]J. D. Beaudoin, B. R. Calder, J. Hiebert, and G. Imahori, "Estimation of sounding uncertainty from measurements of water mass variability," Int. Hydrogr. Rev. **2**, 20–38 (2009).